A Viscoplastic Model of Expanding

Cylindrical Shells Subjected to

Internal Explosive Detonations

Los Alamos
NATIONAL LABORATORY

*A Viscoplastic Model of Expanding
Cylindrical Shells Subjected to
Internal Explosive Detonations*

Rick L. Martineau

Los Alamos
N A T I O N A L   L A B O R A T O R Y

Los Alamos, New Mexico 87545

ACKNOWLEDGMENTS

TABLE OF CONTENTS

List of Tables

List of Figures

LIST OF SYMBOLS AND THEIR DIMENSIONS

U_s –   Shock Velocity [L/T]

U_p –   Particle Velocity [L/T]

P –   Pressure [M/LT^2]

P_H –   Pressure on Hugoniot Curve [M/LT^2]

ρ –   Density [M/L^3]

V –   Specific Volume [L^3/M]

η –   First Strain Invariant [None]

λ –   Lamé Constant [M/LT^2]

G –   Shear Modulus [M/LT^2]

K –   Bulk Modulus [M/LT^2]

D –   Elastic Constant Matrix [M/LT^2]

f –   Void Volume Fraction [L^3/L^3]

f_c –   Critical Void Volume Fraction [L^3/L^3]

f_f –   Final Void Volume Fraction [L^3/L^3]

f_N –   Volume Fraction for Void Nucleation [L^3/L^3]

S_N –   Standard Deviation for Void Nucleation [None]

$\dot{f}_{gr}$ –   Void Growth [L^3/L^{3}T]

$\dot{f}_{nucl}$ –   Void Nucleation Rate [L^3/L^{3}T]

σ_f –   Flow Stress [M/LT^2]

σ_y –   Yield Stress [M/LT^2]

σ_n –   Normal Stress [M/LT^2]

σ_t –   Transverse Stress [M/LT^2]

σ_{ij} –   Stress Tensor [M/LT^2]

σ –   Effective Stress [M/LT^2]

S_{ij} — Deviatoric Stress Tensor $[M/LT^2]$

δ_{ij} — Kronecker Delta [None]

$\dot{W}_p$ — Rate of Plastic Work $[ML^2/T^2]$

T — Temperature $[\theta]$

T_s — Shock Temperature $[\theta]$

Y — Yield Stress $[M/LT^2]$

τ_{max} — Maximum Shear Stress $[M/LT^2]$

C_e — Longitudinal Elastic Wave Speed $[L/T]$

C_{pl} — Plastic Wave Speed $[L/T]$

C_o — Isentropic Sound Speed $[L/T]$

γ — Grüneisen Gamma [None]

η — Normal Strain [None]

ε_V — Volumetric Strain [None]

ε — Strain [None]

ε^{el} — Elastic Strain [None]

ε^{pl} — Plastic Strain [None]

$\dot{\varepsilon}$ — Strain Rate $[1/T]$

$\bar{\varepsilon}_m^{pl}$ — Mean Plastic Strain [None]

E — Energy $[L^2/T^2]$

Q — Heat $[L^2/T^2]$

W^{pl} — Plastic Work $[L^2/T^2]$

C_v — Constant Volume Specific Heat $[L^2/T^2\,\theta]$

S — Specific Entropy $[L^2/T^2\,\theta]$

ϕ — Yield Function [None]

ζ — Relative Material Density $[ML^3/ML^3]$

Unless otherwise noted, the letter 'd' preceding a symbol indicates the incremental value.

A VISCOPLASTIC MODEL OF EXPANDING CYLINDRICAL SHELLS

SUBJECTED TO INTERNAL EXPLOSIVE DETONATIONS

by

Rick L. Martineau

ABSTRACT

Magnetic flux compression generators rely on the expansion of thin ductile shells to generate magnetic fields. These thin shells are filled with high explosives, which when detonated, cause the shell to expand to over 200% strain at strain-rates on the order of 10^4 s^{-1}. Experimental data indicate the development and growth of multiple plastic instabilities which appear in a quasi-periodic pattern on the surfaces of the shells. These quasi-periodic instabilities are connected by localized zones of intense shear that are orientated approximately 45° from the outward radial direction. The quasi-periodic instabilities continue to develop and eventually become through-cracks, causing the shell to fragment.

A viscoplastic constitutive model is formulated to model the high strain-rate expansion and provide insight into the development of plastic instabilities. The formulation of the viscoplastic constitutive model includes the effects of shock heating and damage in the form of microvoid nucleation, growth, and coalescence in the expanding shell. This model uses the Johnson-Cook strength model with the Mie-Grüneisen equation of state and a modified Gurson yield surface. The constitutive model

includes the modifications proposed by Tvergaard and the plastic strain controlled nucleation introduced by Needleman. The constitutive model is implemented as a user material subroutine into ABAQUS/Explicit, which is a commercially available non-linear explicit dynamic finite element program. A cylindrical shell is modeled using both axisymmetric and plane strain elements.

Two experiments were conducted involving plane wave detonated, explosively filled, copper cylinders. Instability, displacement, and velocity data were recorded using a fast framing camera and a Fabry-Perot interferometer. Good agreement is shown between the numerical results and experimental data. An additional explosively bulged cylinder experiment was also performed and a photomicrograph of an instability is shown to provide a qualitative comparison between the experimental observations and the numerical predictions.

Observations from this research indicate the onset of a quasi-periodic pattern in the through-thickness equivalent plastic strain, which occurs early in the deformation process before the stress waves have attenuated. This quasi-periodic pattern continues to develop, eventually connecting the inner and outer surfaces, at which time quasi-periodic instabilities are observed on the surfaces of the shell. In addition, parameter studies performed as part of this research indicate relationships between the shell thickness, the number of instabilities, and the approximate time to failure.

1.0 Introduction and Problem Definition

The high strain-rate deformation of ductile materials subjected to high dynamic pressures is of great fundamental importance to physicists and engineers. High pressure dynamic loading which results in large impulses with short rise times can generate shock waves in a material. These high pressure shock waves, which are often generated by explosives, can destroy, modify or enhance materials. Experimental data have shown that when ductile shells are subjected to internal pressure loading from high explosives, they experience large plastic deformation prior to fragmenting. These shells expand at strain rates on the order of 10^4 sec^{-1}. At approximately 150% strain, multiple plastic instabilities are observed on the outer surface of these shells in a quasi-periodic pattern. These quasi-periodic instabilities continue to develop and eventually form cracks that progress in a way that causes the shell to break into fragments. The entire process takes less than 100 microseconds from detonation to complete fragmentation.

Developing the modeling and constitutive relationships for predicting these plastic instabilities and the overall deformation of the shell are the motivation for this dissertation. Although others have worked on limited constitutive models demonstrating plastic instabilities on rings and cylinders, few have compared their results with experimental data. An experimentally verified finite element model incorporating the constitutive relationships for large plastic deformation, void growth, inertia, strain-rate,

1

high pressure equation of state effects, and thermal effects will be a valuable tool for analyzing rapidly expanding shells.

1.1 Why Study Expanding Shells

The elastic/viscoplastic behavior of materials is an area of study that encompasses a variety of scientific disciplines with industrial and military applications. Industrial applications typically produce a structure or improve a material. Military applications are generally intended to defeat or protect a structure. In either case, the response of structures subjected to rapidly changing loads is considerably different from those under quasi-static conditions. Applications for this research include hypervelocity accelerators, magnetic flux compression generators, explosive power generating plants, and containment vessels.

In 1948, the first hypervelocity accelerator was developed at the New Mexico School of Mines. This accelerator consisted of a combustion chamber which when ignited, accelerated a solid projectile to velocities as high as 11 km/s. The mechanical behavior of this projectile during the acceleration phases of the machine is critical in understanding the machine limitations (Kinslow, 1970). Scientists at General Electric and the Stanford Research Institute continued this research and in particular investigated applications for explosively driven guns and shaped charges. During the 1980's, research in the area of rail guns became popular as scientists continued to look at hypervelocity accelerators. This work is continuing at the University of Texas (Persad et al., 1997) and at other research institutions around the world. In a recent report by Trucano and Chhabildas, (1995), it was recognized that preventing the fracture and failure of the flier

2

plates which are subjected to extraordinary accelerations is crucial to the functionality of the machine.

A magnetic flux compression generator uses explosives to amplify electromagnetic fields. This device consists of a thin cylindrical shell filled with high explosives and a low inductance coil (Prishchepenko, 1994). Understanding the high-strain-rate expansion and deformation of the shell is important in improving the functionality and reliability of this type of generator.

Several countries including the USA, Russia, Japan, and UK are working on explosive generator plants (Shchegolevskii, 1983). While this process does not involve the large plastic deformation of materials, understanding the dynamic response of materials is important in the design of the hardware used to contain the explosive detonations.

Large thin walled vessels are often used to contain high explosive detonations in the reduction and elimination of high explosive materials. Police and antiterrorist personnel around the world rely on these vessels to save lives and eliminate potential hazards. Containment vessels are also important in the design and operation of nuclear power plants. These vessels are re-used many times and may sustain damage. Predicting the damage, structural integrity, ultimate load capability, and remaining life are important applications for which the research of this dissertation is needed. A detailed understanding of the dynamic response of the material in the plastic region of behavior is critical to ensure structural integrity.

An understanding of the dynamic response and high strain-rate behavior of materials is also important for other applications. In space, micrometeorites can travel at

velocities as high as 30 km/sec before impacting space structures. Damage to these structures may result from the impact itself, shock waves, or excitation of destructive vibrational modes.

The energy associated with shock waves is also instrumental in industry to harden materials. Techniques like explosive hardening and explosive forming are important in the production of large complex parts. Materials undergoing large plastic deformation at high strain-rates demonstrate enhanced formability allowing engineers to design and produce complicated structures and moldings. Industry also relies on the dynamic behavior of materials to explosively weld dissimilar metals. More recently, explosives are being used for shock synthesis and shock consolidation. Shock synthesis is used to produce diamond powder from carbon, while shock consolidation uses the energy of shock waves to bond fine metal powders.

There is an ongoing need to understand the behavior of materials subjected to high strain-rate deformation. Numerical models capable of predicting the deformation and failure of materials subjected to high strain rates could substantially reduce costs and improve structural reliability. The research presented here provides an investigation into developing this capability for ductile materials such as oxygen free electronic (OFE) grade copper.

The strain rates of interest in this investigation are on the order $10^4\,s^{-1}$, which are easily obtainable with conventional high explosives. Meyers (1994) described five strain-rate categories. These categories are presented below in Table 1.1.

Table 1.1: Classification of Strain-Rates and Testing Methods

Strain-rate, s^{-1}	Category	Testing Method
$10^7 - 10^5$	Ultra High Velocity Impact	Explosives, Impact, Laser
$10^5 - 10^3$	Dynamic-High	Explosives
$10^3 - 10^0$	Dynamic-Low	High Velocity Machines
$10^0 - 10^{-5}$	Quasi-Static	Hydraulic, Screw Driven Machines
$10^{-5} - 10^{-9}$	Creep and Stress Relaxation	Conventional Testing Machines

Materials research in the Dynamic-Low, Quasi-Static, and Creep categories is fairly advanced. However, research in the Dynamic-High and Ultra-High areas is still in its infancy, further justifying the scientific importance of this study.

High explosives are typically used to obtain strain rates above 10^3 s^{-1} and at sufficiently high strain-rates; material can behave like a fluid. Shock physicists, who thoroughly understand the high explosive detonations, have sometimes underestimated the importance of classical engineering plasticity in the high strain-rate deformation of solid materials. This has resulted in the use of hydrocodes to analyze the deformation process. Hydrocodes typically treat the material as a fluid and assume shear effects are negligible or in some cases model the behavior of the material without strength. A summary of previous experimental and numerical work regarding the expansion of thin shells and their failure is provided in the next two sections.

1.2 Background on Experimental Studies

When a thin-walled circular cylinder is subjected to an internal explosion, the walls of the cylinder expand radially. For ductile materials this radial expansion occurs at very high velocities prior to failure by fragmentation. In 1943, Gurney (1943) derived a widely used model for predicting the terminal velocities of fragments from shells

subjected to internal explosive detonations. His expression is based on an energy balance that assumes the potential energy characterizing the explosive charge before the detonation is equal to the kinetic energy of the gases from the detonation products and the metal after detonation and expansion. Gurney's model provides an equation for determining the terminal velocity of common configurations, but provides no information regarding the deformation process itself. In addition, his model does not consider the energy consumed in the deformation of the shell.

The failure of cylindrical structures was first examined in 1944 as a fragmentation problem by Taylor (1963a). G. I. Taylor was concerned with the formation of longitudinal cracks on the outer surface of cylindrical shells subjected to an internal explosive detonation. Taylor proposed that longitudinal cracks in the axial plane will open out into regions where the circumferential stress is tensile, but will not penetrate into regions where this stress is compressive. He concluded that the cracks will not penetrate to the inner wall of the cylinder until the compressive region is reduced to zero thickness and in some cases, the cylinder has nearly doubled its initial diameter. In addition, Taylor observed that for copper tubes with a 3.8 mm wall thickness, the hoop strain at failure by fragmentation was on average 2.4. The research presented in this dissertation is compared with Taylor's conclusions and observations. An expanding circular ring illustrating Taylor's conclusions is shown below in Figure 1.1, where P, represents the internal pressure, t the shell thickness, and r the expanded radius.
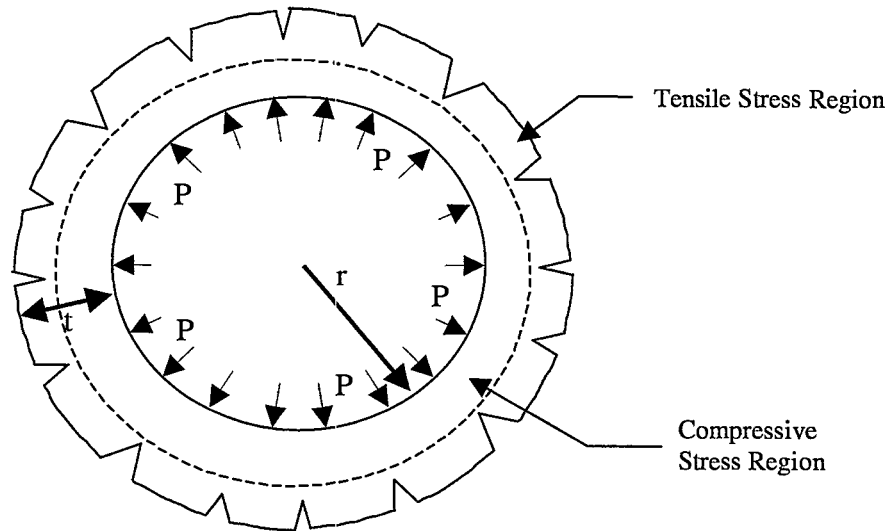
Figure 1.1: Compressive and Tensile Stresses on Expanding Ring

About the same time, Mott (1947), attempted to predict the distribution and size

of fragments from a tubular structure based on the assumptions of a perfectly plastic

material model and probability theory. Mott examined fragments from expanding shells

and concluded that considerable plastic deformation occurs prior to case fragmentation.

He also concluded that by the time fracture occurs, the case is traveling at some terminal

velocity and the internal pressures for the high explosive have dropped to a small fraction

of their original value. Mott observed two types of fractures; shear fractures and cup and

cone type fractures. Mott also concluded that initiation of the fracture is not necessarily a

surface phenomenon as reported by Taylor, but may occur inside the wall of the shell as

in the case of a tensile specimen where high triaxial tensile stress causes the initiation of

fracture.

G. I. Taylor (1963b) continued his research in this area and in 1963, another paper

was published on the expansion of cylindrical shells detonated on one end. In this paper,

Taylor developed analytical expressions for estimating the velocity profile of the shell.

In 1967, Slate and others (Slate et al., 1967) experimentally examined the behavior of several thin spherical shells subjected to internal explosive detonations. These shells were fabricated from various materials including copper, aluminum, and titanium. Their report indicated that for copper shells with a thickness to radius ratio of 0.02, the shells fragmented early with the formation of bubbles on the surface indicating a fluid like response. A more ductile response occurred for a radius ratio of 0.04. At this ratio, they observed what appeared to be local thinning between the fragments before the detonation products pierced through the surface. Finally, a more brittle response was observed for copper shells with a ratio of 0.08. At this ratio, the surface ripples became more obvious and eventually these ripples developed into lines of fracture. They felt this pattern was a result of heterogeneities in the density or crystalline structure of the material, thus providing a potential pattern for rupture under circumferential strain. In summary, their observations indicate that the thicker the shell, the more evident the surface cracking and in addition, the higher the strain to rupture.

Hoggatt and Recht (1968) furthered the experimental study of fragmenting cylinders and developed a mathematical model assuming the fractures occur along lines of maximum shear. In addition, Hoggatt and Recht observed different types of fractures based on the amount of HE and the detonation pressures. At low detonation pressures, deep cracks formed on the outer surface before unstable shear zones began to develop. This resulted in fragments with deep radial cracks on the surface and shear zones only near the inner diameter. Hoggatt and Recht define shear zones as cracks that lie along shear planes, which are rotated approximately 45 degrees from the outward radial direction. At high detonation pressures, the compressive hoop stress from the detonation

retards the growth of cracks and the unstable shear zones form earlier. As a result, larger

shear zones are observed on the fragments. An illustration of the fracture resulting from

a high and low pressure detonation is shown in Figure 1.2

<div align="center">High Pressure Detonation   Low Pressure Detonation</div>

Figure 1.2: Exaggerated Fractures from a High and Low Pressure Detonation

Later, Al-Hassani and others (1969a) determined from experiments that the radial

expansion of the vessel walls continues long after attenuation of the shock waves in the

material. In addition, they provide an analytical expression for the hoop and radial stress

in the vessel wall assuming a perfectly plastic material and confirmed the behavior

observed by Taylor. In a separate report by Al-Hassani and Johnson (1969b), they

concluded that the strain-rate, strain hardening, and deformation induced temperature are

important to the yield behavior and that they influence both the fracture radius and

velocity, although they did not include them in their analysis.

Wesenberg and Sagartz (1977) analyzed the expansion of thin cylindrical shells

at strain rates of 10^4 sec^{-1}. They discuss the radial expansion of the cylinders and their

subsequent fracture by providing a numerical solution to Mott's fracture equation (Mott,

1947). Wesenberg and Sagartz compared Mott's probabilistic analysis with experimental

<div align="center">9</div>

data, which were reasonably close. They also observed that the number of fragments decreases with material density and decreasing strain-rate or detonation pressure.

The research presented in this dissertation will verify G. I. Taylor's conclusions and observations regarding failure and the tensile and compressive stress regions in an expanding shell. Reports by Mott, Slate, Hoggatt, Recht, and others indicate fragment variations are based on material thickness or detonation pressures. This dissertation will also provide numerical and experimental results for cylinders of different thicknesses, which will dispute or confirm the thickness dependent effects observed by Mott, Slate, Hoggatt, and Recht.

1.3 Background on Numerical Studies

In the late 1970's experimental research into the high strain-rate expansion of explosively loaded shells began to taper off. Experiments probably became more costly and the advent of the super computer provided a numerical means to investigate the high strain-rate expansion phenomena. As a result, scientists conducted more numerical studies in an effort to understand the development of plastic instabilities in dynamically loaded structures and dynamic fragmentation. Early numerical studies were limited to the expansion of rings and axially detonated cylinders. In both of these cases the entire geometry expands uniformly in the radial direction in the absence of a longitudinal stress component. The research presented in this dissertation considers this and the more complicated end detonated cylinder where the expansion varies along the longitudinal axis of the cylinder.

Early results by Hoggatt and Recht (1968), suggest that thermoplastic instabilities occur when the local flow stress decreases with increasing strain. This occurs when the rate of thermal softening exceeds the rate of work hardening. In general, the loss of stability is assumed to take place when an increment in strain occurs with no simultaneous increase in pressure or load (Duffey, 1989). Duffey examined the effects of work hardening and mentions that work hardening effectively spreads out the deformation to a point that prevents strain localization. Neglecting inertia effects, materials with greater strain hardening exhibit higher instability strains.

A formulation for modeling dynamic plastic instabilities in a thin sheet was developed by J. W. Taylor (Taylor et al., 1978). Their approach is based on hydrodynamic principles where they assume that the shear effects are negligible. They introduced a thickness perturbation in thin sheets and demonstrated that the size and appearance of the instabilities are dependent on the strain-rate and work hardening. Their analysis does not include porosity or temperature effects, nor does it consider multi-axial stresses.

In 1983, Johnson (1983) examined the ductile failure of rapidly expanding rings. Johnson describes the time dependent heterogeneous plastic deformation in terms of the differential equations of thermoplasticity, conservation of mass, and conservation of momentum. Johnson's model uses a small perturbation in the wall thickness or porosity to create the instability. He also examines the influence of work hardening and thermal softening and suggests that thermal effects can not be ignored. However, Johnson's constitutive model focuses on the response of the material using a high pressure equation of state formulation and not the accepted theory of plasticity. In addition, his paper

considers only the one-dimensional case and thus can not be easily extended to cylindrical shells under a multi-axial state of stress.

Anderson, Predebon, and Karpp (1985) developed a two-dimensional finite difference code to model expanding cylinders. They felt typical hydrodynamic codes over-predicted the fragment velocities and attempted to obtain a more complete solution. Their model includes gas leakage and results for the velocity and expansion angle are compared with experimental data. However, their model assumes elastic-perfectly-plastic material behavior and does not consider instabilities.

In 1997, Hao and Brocks (1997) implemented a void nucleation and growth constitutive model into a numerical finite element code. The constitutive model they developed was written as a user subroutine for the ABAQUS/Standard code. Their model was capable of analyzing low strain-rate problems involving creep and quasi-static type loading, rather than the high strain-rate problems considered in this dissertation.

1.4 Shortcomings in Existing Literature

Considering the results of the literature cited here, it is clear that strain-rate, material density, temperature, and inertial effects are important in large strain plastic deformation and development of instabilities when materials are subjected to high strain rates. These instabilities may result from inadequate thermal diffusion and excessive plastic flow and may include the effects of damage in the material. Several authors have examined instabilities associated with both uniaxial and bi-axial stress under quasi-static conditions, but most have not considered materials subjected to multiaxial stress states at strain rates on the order of 10^4 s^{-1}.

The previous experimental and numerical work leaves several shortcomings. In the early literature, the material used in experiments was not carefully characterized or documented. As a result, little is known about the grain size and hardness of the materials used, which makes it difficult to duplicate experimental results. The size of copper grains can be quite large resulting in perhaps one grain through the thickness of the tube. The microstructure, particularly the hardness and number of grains through the thickness of the tube, could significantly affect high strain-rate deformation. The work presented here examines the microstructure of the material before and after the experiment.

Much of the current numerical literature only considers one stress component or at most the trace of the stress tensor. Furthermore, the geometries considered in the current literature are typically one-dimensional. The research presented here considers the entire stress and strain tensor according to the fundamental constitutive formulations for three-dimensional plasticity. This complexity advances the current state of the art. In addition, it allows researchers to consider not only the complex expansion of shells, but also provides the foundation to examine large strain plastic instabilities.

From a review of the numerical literature, very few authors have included the high pressure equation of state effects, which could be important in the formulation of the constitutive equations. Those that have included these effects examined situations with strain rates much higher than 10^4 sec^{-1} or provided formulations that are limited to one-dimensional calculations. Most of the authors who have implemented equation of state type formulations are typically concerned with 1-dimensional fragmentation or spall and do not focus on the evolution of large strain plastic instabilities.

In some cases, researchers have neglected the strength of the material, which could be significant for predicting instabilities for rapidly expanding shells. In other cases, they assume a perfectly-plastic material where the flow stress is constant and the strength model for the material is independent of the material behavior. The strength model typically relates the current state of the material, most often strain, to some allowable state of stress. Numerous strength models exist in the current literature and a few of them are examined in Chapter 2. The Johnson-Cook strength model is arguably the most widely used in both the previous and current literature for high strain-rate plasticity. The underlying principles of the Johnson-Cook model and its implementation are discussed in Chapters 2 and 3.

Shock physicists contend that numerical codes can not completely characterize the shock front or detonation front due to processor limitations even with the world's fastest super computers. However, this research is not concerned with the microscopic behavior at either front, but rather treats the materials as a continuum and is concerned only with the average microscopic behavior. Curran et al. (1987) describe the average microscopic behavior in terms of state variables in the constitutive relations of materials. This continuum mechanics approach is referred to as "Microstatistical Fracture Mechanics" (MSFM).

The MSFM approach is considered in the development of the damage model. Damage, which results from the effects of microdefects in the material, is incorporated in the form of a void model. This void model includes the effects of microvoid nucleation, growth, and coalescence in the material and is an important aspect in this constitutive model. In summing up the current literature, no one has formulated a model that includes

the 3-dimensional fundamental equations for high strain-rate plasticity with a high pressure equation of state model, a microvoid damage model, and a high strain-rate material strength model to study the expansion of thin ductile shells.

1.5 Scope of Work Presented in this Dissertation

The purpose of this research is to develop an experimentally verified finite element model capable of predicting the high strain-rate expansion of explosively loaded cylindrical shells. In addition, the constitutive model developed in this research provides insight into the initiation and development of plastic instabilities on the surfaces of the shell. The constitutive model is based on the Johnson-Cook strength model, Mie-Grüneisen equation of state (EOS) model, and the GTN or modified Gurson void model.

The constitutive model is verified with experimental data from two plane wave detonated copper cylinders filled with high explosive. The material for these cylinders is carefully characterized and state-of-the-art diagnostic equipment is used to record the cylinder wall displacement and velocity during the experiments.

The numerical model is written to allow future modifications to the constitutive equations and additional damage criteria. The model is multi-dimensional and assumes void nucleation and growth is the main damage mechanism leading to the onset of plastic instabilities. As with most Lagrangian finite element models, the accuracy of the of the results diminishes with large element distortions and as a result the user must be cautious of extensive element warping, strain, and aspect ratios. In addition, the explicit finite element code used in this research limits the user to single integration point elements and as a result requires high mesh densities. At strain rates above 10^6 s^{-1}, the accuracy of the

Johnson-Cook model tends to diminish and result from this numerical model may no longer be accurate. Finally, this is a newly developed model and further limitations may be observed as the code is exercised with new applications.

The remaining chapters of this dissertation focus on the numerical model, the experimental and numerical results, and the onset of instabilities. Chapter 2 discusses the constitutive equations used in the development of the numerical model. The implementation of the constitutive equations in the numerical model is discussed in Chapter 3. Chapter 4 discusses the material characterization and set-up of the experiment used for verifying the numerical model. A comparison of experimental data with the results from the numerical model is provided in Chapter 5. Chapter 6 focuses on the development of the quasi-periodic instabilities for cylinder of different thickness. Finally Chapter 7 provides a summary, a list of conclusions, and recommendations for future work.

2.0 Constitutive Models

Typical hydrodynamic calculations neglect the strength of the material and treat the material as a fluid. This simplification is reasonable in the case of fluids or solids undergoing high compression shocks resulting in a fluid type behavior. The copper cylinders considered in this study are subjected to high pressures, but are not believed to behave as a fluid. Instead, as the material strains, thermal energy is deposited in the material as a result of shock loading and plastic work. This thermal energy has an effect on the flow surface and resultant stress state of the material. In addition, damage accumulates in the material as it yields. This damage, which is modeled in the form of microvoids accumulating in the material, leads to the onset of the instabilities in the material. Recent literature suggests that constitutive models for modeling this high strain-rate behavior should be composed of at least three models: a strain-rate and temperature dependent material strength model, an equation of state, and a microvoid damage model. The research presented here includes all three of these models.

This chapter is divided into three sections. Each section discusses or formulates a particular part of the constitutive model used to describe the deformation of the expanding cylindrical shells. The first section describes the material strength model, which predicts the flow stress of the material based on temperature, strain, and strain-rate. The second section provides an overview of the shock and stress waves propagation in solids and presents the background information regarding the equation of state, Rayleigh

line, and Hugoniot curve. In addition, this section formulates the equations used to model the shock wave effects on the bulk modulus and material temperature. The third section provides an overview of the damage model. The damage model used in this work is based on the nucleation, coalescence, and growth of microvoids in the material as a result of plastic strain.

2.1 Material Strength Models

Several strength models exist in the current literature. Strength models like the Zerrilli-Armstrong and Mechanical Threshold Stress (MTS) model are considered to be physically based models, while the Johnson-Cook model is an empirically based model. Numerous experiments have been conducted using each of these models, and all show reasonable agreement for dynamic strain rates below 10^5 s^{-1}.

Zerilli and Armstrong proposed a microstructural based constitutive model based on the framework of thermally activated dislocation motion (Zerilli and Armstrong, 1986). Their model results in equations that are very similar to the stress function proposed by Hall (1951) and Petch (1953) and contains terms for the flow stress, the grain size dependence, and a stress correction factor that is slightly different for FCC and BCC metals. For FCC metals the correction factor couples the plastic strain with the strain rate and temperature, while for BCC metals, the plastic strain is uncoupled from the strain rate and temperature.

The Mechanical Threshold Stress Model (Follansbee and Kocks, 1988) uses the same concepts as the Zerilli-Armstrong Model. In the MTS model, the thermally activated dislocation interactions are described by the linear summation of three different

18

terms. The first term represents the internal stress resulting from the dislocation interactions, perhaps with grain boundaries. The second term represents the strain rate and temperature effects on the yield stress. The final term represents the dislocation interactions from deformation and accounts for work hardening and thermal softening.

A number of empirically based strength models have been proposed in the literature, and most of these show reasonable agreement with experimental data. Typically, these models define the flow stress as some function of strain raised to a power. Johnson and Cook (1983) used this principle in formulating their model. The strength model presented by Johnson and Cook has five experimentally determined parameters (A, B, C, n, m) coupled together in an easily identified form. Their model expresses the flow stress as a function of the equivalent plastic strain, strain rate, and temperature. The Johnson-Cook equation for the flow stress is expressed as

$$\sigma_f = \left(A + B\varepsilon^n\right)\left(1 + C\ln\dot{\varepsilon}^*\right)\left(1 - T^{*m}\right), \tag{2.1}$$

where ε is the equivalent plastic strain,

$$\dot{\varepsilon}^* = \frac{\dot{\varepsilon}}{\dot{\varepsilon}_o}, \tag{2.2}$$

is the dimensionless plastic strain-rate for a reference strain-rate $\dot{\varepsilon}_o = 1.0 \text{ s}^{-1}$ and

$$T^* = \frac{\left(T - T_{room}\right)}{\left(T_{melt} - T_{room}\right)} \tag{2.3}$$

is what Johnson and Cook refer to as the homologous temperature.

The five material constants in eqn. (2.1) are separated into three multiplicative terms. The first term in eqn. (2.1) represents the strain hardening with A interpreted as the initial yield stress, B the strain hardening coefficient, and n the strain hardening

exponent. The second term in eqn (2.1) represents the strain-rate effect with C interpreted as the strain-rate hardening coefficient. The last term in eqn. (2.1) represents the thermal softening with m interpreted as the thermal softening exponent. The five material constants A, B, C, n, and m were determined by Johnson and Cook from a series of tensile and torsion tests evaluated at various temperatures and strain rates ranging from 10^3-10^5 s^{-1} (Johnson and Cook, 1983). Specific values for these constants as reported by Johnson and Cook are given in Table 2.1. Strain-rate dependent plots of the adiabatic flow stress from eqn. (2.1) as function of strain are shown in Figure 2.1 for OFE (Oxygen-Free Electronic) copper. Adiabatic effects were accounted for in eqn (2.1) by including the increase in temperature resulting from plastic work. The formulation for this increase in temperature is discussed later in this chapter.

Table 2.1. Material Constants for the Johnson-Cook Strength Model

Material	A (MPa)	B (MPa)	n	C	m
OFE Copper	90	292	0.31	0.025	1.09
Cartridge Brass	112	505	0.42	0.009	1.68
Nickel 200	163	648	0.33	0.006	1.44
Armco Iron	175	380	0.32	0.060	0.55
1006 Steel	350	275	0.36	0.022	1.00
2024-T351 Aluminum	265	426	0.34	0.015	1.00
7039 Aluminum	337	343	0.41	0.010	1.00
4340 Steel	792	510	0.26	0.014	1.03
Tungston Alloy	1506	177	0.12	0.016	1.00
S-7 Tool Steel	1539	477	0.18	0.012	1.00
Uranium-.75Ti	1079	1120	0.25	0.007	1.00
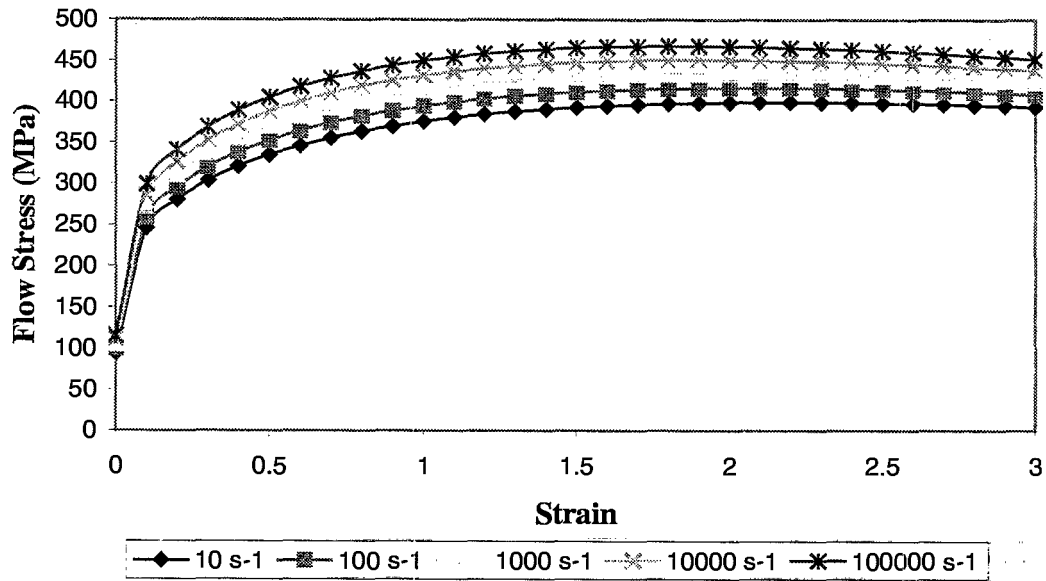
Figure 2.1: Johnson-Cook Flow Stress for OFE Copper as a Function of Strain

The Johnson-Cook model (Johnson and Cook, 1983) has several desirable features. One of the most obvious is its ease of implementation. In addition, it can be readily applied to a variety of materials and the constants are easily obtainable for several materials of interest. The effects of various parameters in the equations are easily identifiable and the Johnson-Cook strength model does not require an extraordinary amount of computer time. However, since it has no physical basis, caution must be used when extrapolating ε, $\dot{\varepsilon}$, and T beyond the limits of the data from which the constants were determined. The equations and implementation of the Johnson-Cook model into the plasticity model will be further examined in Chapter 3.

2.2 Shock Waves and the Equation of State

Shock wave studies examine the behavior of materials that are subjected to intense short term loading which forces the material into states not usually encountered.

The pressures attained from this loading can be two orders of magnitude larger than those attainable by conventional methods (Skidmore, 1965). This loading is typically a result of explosive detonations, the duration of which is on the order of microseconds. High speed diagnostic equipment is required to experimentally observe shock waves and as a result investigations in this area are limited.

The study of shock waves in solids was first introduced in the UK by Pack and others in 1948 (Pack et al. 1948). Later in 1955, similar work was reported in the USA by Gorason et al. (1955). In addition, Walsh and Christian (1955) made significant contributions in this area while working at Los Alamos National Laboratory. During the 1960's scientists began focusing on shock waves resulting from high velocity impact (Duvall, 1961). Interest in shock waves has recently expanded in industry as engineers recognize the value of using explosive techniques for welding and plastic forming. In addition, metallurgists are studying the changes in the microstructure of solids following intense transient loading. Intense quantities of energy are deposited into materials from shock loading. This energy and the resulting temperatures are included as an integral part of the work presented in this study.

Arguably, when the solid is subjected to intense hydrodynamic forces, the shear stresses are relatively small, and the stress system is effectively hydrostatic (Skidmore, 1965). Therefore, the effects of shear stress are typically not included in hydrodynamic methods and it is possible to treat the material as a fluid when attempting to understand shock wave propagation in solids. The fundamental requirement for establishing a shock wave is that the velocity of the disturbance increases with an increase in pressure.

Understanding of the concept of shock wave propagation in a material can be aided by considering the simplified analogy of the flow of snow in front of a snowplow. As the snowplow moves into a fresh new snow, a layer of packed snow begins to build up in front of the plow. The snow immediately in front of the blade of the snowplow travels faster than the snow further ahead of the blade. Eventually the wave front becomes infinitely steep, forming a mathematical discontinuity (Graham, 1993). This discontinuous wave front is called a shock wave.

In a shock wave, the material changes discontinuously from one side of the front to the other and the expressions governing sound wave behavior are no longer strictly applicable. Instead scientists use what are called the Rankine-Hugoniot relations or jump conditions. A schematic of the profile of shock front is shown below in Figure 2.2 where U_s is the shock velocity, U_p is the particle velocity, ρ is the density of the material, E is the energy, and P is the pressure. The subscript 'o' indicates the properties of the material ahead of the shock front.
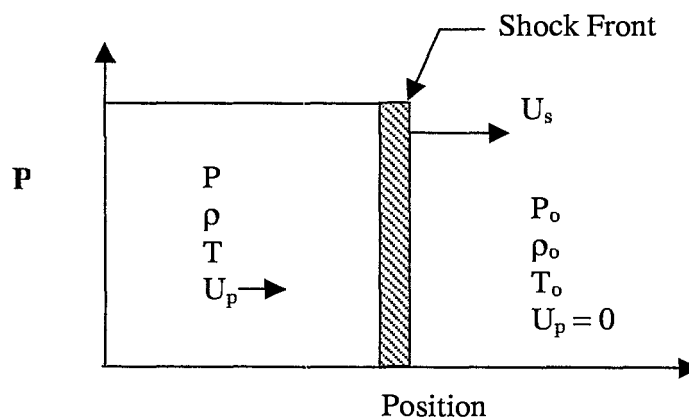
Figure 2.2: Profile of a Shock Front Propagating Through a Material

The useful form of Rankine-Hugoniot relations result from writing the conservation equations in their discrete forms. The conservation of mass becomes,

$$\rho_0 U_s = \rho \left(U_s - U_p \right). \tag{2.4}$$

While the conservation of energy becomes,

$$E - E_o = \frac{1}{2}(P + P_0)(V_0 - V), \tag{2.5}$$

and the conservation of momentum becomes,

$$P - P_o = \rho_o U_s U_p. \tag{2.6}$$

This results in three equations and five unknown parameters.

A fourth equation known as the equation of state (EOS) is necessary to determine any of the parameters as a function of one parameter. The EOS, which will be discussed later, defines all of the equilibrium states that can exist in a material. If the state of the material behind the shock is an equilibrium state, then it too satisfies the EOS. If both the Rankine-Hugoniot conditions and the EOS are satisfied simultaneously, then the energy terms between them may be eliminated and it is possible to obtain a P-V (Pressure-Volume) relation that is unique for the material represented by the EOS. The curve represented by this relation is called the Hugoniot curve, which simply represents a unique curve in the P-V plane representing the locus of all shocked states attainable behind the shock.

The conservation of momentum defines a straight line of slope $(P - P_0) / (V - V_0)$ in the P-V plane. This line is called the Rayleigh line. A graphical representation of the Hugoniot curve, and Rayleigh line is shown in Figure 2.3. The adiabats in Figure 2.3 represent lines of constant entropy on the pressure-volume plane.
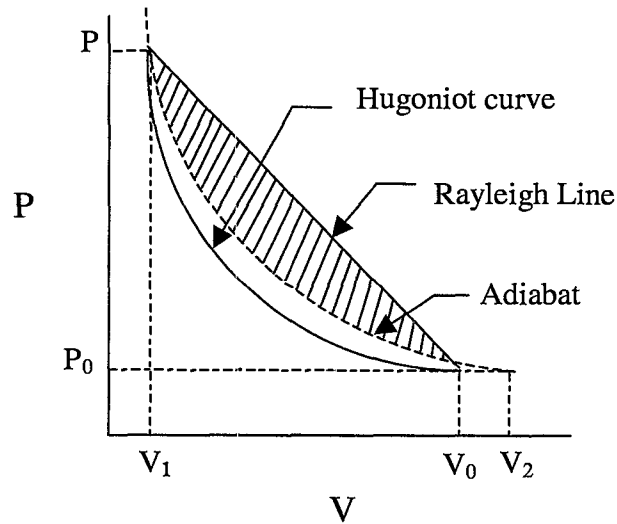
Figure 2.3: Plot of the Hugoniot Curve and Rayleigh Line on the P-V Plane

When the pressure in the shock front is increased, it does not follow the adiabat or

the Hugoniot Curve. Instead it follows along the Rayleigh line from P_0 to P. The

unloading process behind the shock front is usually assumed to be adiabatic and as result

takes place along the adiabatic curve from V_1 to V_2. The initial specific volume, V_o, is

different than V_2 due to an increase in the temperature from the energy deposited in the

material. The irreversibility of the process is shown graphically in Figure 2.3 as the

hatched area between the Rayleigh line and the release adiabat. In practice, physicists

often assume the unloading takes place along the Hugoniot. This is a reasonable

approximation since the Hugoniot and the adiabat have close proximity. However, recall

the Hugoniot curve represents the locus of end states, not the shock path.

The concept of shock stability is important in understanding wave propagation in

a material. Using an "Eulerian" coordinate system, consider a compression wave

resulting from two small compressional disturbances as shown in Figure 2.4.
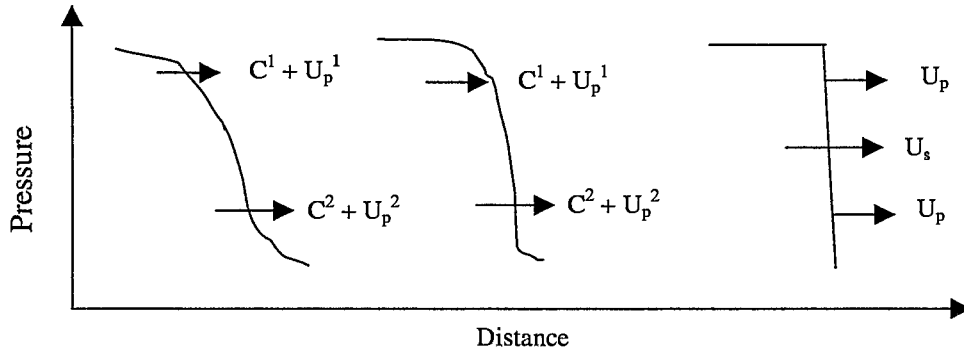
Figure 2.4: Formation of a Stable Shock Wave

The first wave moves at a speed of $C^1 + U_p^1$, where C^1 is the pressure dependent sound speed. The second wave moves at a speed of $C^2 + U_p^2$ where again C^2 is the local sound speed. In general, the local sound speed of a material increases with pressure. The high pressure wave travels faster than the low pressure wave so that the combined compression wave becomes steeper. Eventually, the first wave overtakes the second. This results in a discontinuous disturbance or shock wave, which travels at the speed U_s. In general, for a stable shock to exist, the velocity of the disturbance, $C + U_p$, must always be greater than or equal to the shock velocity, U_s. Otherwise, the disturbance will not be able to catch up to the shock and the shock will decay, develop an elastic precursor, or cause a phase transformation in the material. Thus a necessary condition for shock stability is

$$U_p + C \geq U_s .$$
(2.7)

Three different stress wave configurations can exist in a solid and understanding the Rayleigh line and Hugoniot curve provides insight into the structure of the wave. Consider the stress system behind a one-dimensional compressive stress wave where the volumetric strain, ε_v which is defined as positive in compression, is described by

$$\varepsilon_v := \frac{V_0 - V}{V_0} = 1 - \frac{V}{V_0}, \tag{2.8}$$

for small strain elasticity. The normal and transverse elastic stress for an element subjected to uniaxial strain can be respectively written as

$$\sigma_n = (\lambda + 2G)\,\varepsilon_v \tag{2.9}$$

and

$$\sigma_t = \lambda\,\varepsilon_v \tag{2.10}$$

where λ is the Lamé constant and G is the shear modulus. The Lamé constant is related to the bulk modulus, K, (Love, 1944) as

$$\lambda = K - \frac{2}{3}G. \tag{2.11}$$

For the case of hydrostatic pressure, P, the bulk modulus can be defined as

$$K = \frac{P}{\varepsilon_v}. \tag{2.12}$$

Using eqns. (2.9), (2.10), and (2.11), the equations for the elastic response of the material can now be written as

$$\sigma_n = \left(K + \frac{4}{3}G\right)\varepsilon_v \tag{2.13}$$

and

$$\sigma_t = \left(K - \frac{2}{3}G\right)\varepsilon_v. \tag{2.14}$$

These elastic relations remain valid provided the yield criterion is not violated. In this case, the yield criteria can be written in terms of the maximum shear stress as

$$Y = 2\tau_{max} = (\sigma_n - \sigma_t), \tag{2.15}$$

When yielding occurs, $\left(\sigma_n - \sigma_t\right)$ remains constant and as a result,

$$\sigma_n - \sigma_t \leq Y. \tag{2.16}$$

or

$$2G\varepsilon_v \leq Y \tag{2.17}$$

Combining eqn. (2.12), (2.13), and (2.17), the normal yield stress, σ_y, can be written as

$$\sigma_y = P + \frac{2}{3}Y \tag{2.18}$$

The stress wave behavior of a material subjected to shock loading can be understood with these equations. First consider the plot of stress vs. strain shown in Figure 2.5. This plot is similar to the plot shown by Skidmore (1965).
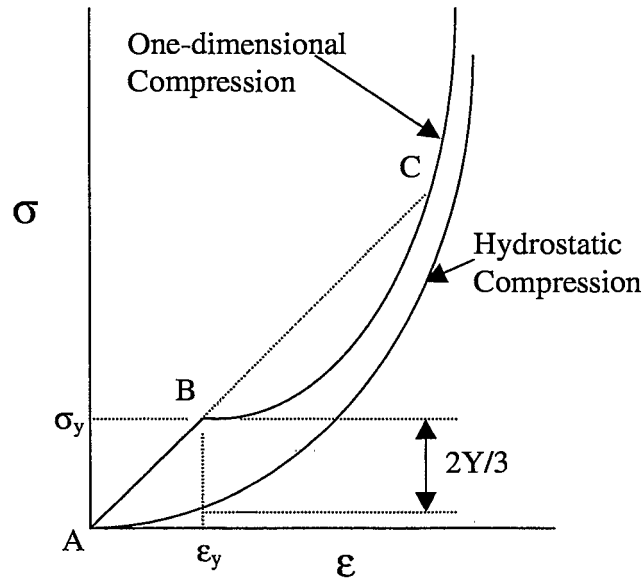
Figure 2.5: One-dimensional and Hydrostatic Compression of Solids

Point B in Figure 2.5 is called the Hugoniot Elastic Limit (HEL). The stresses below this limit are elastic and propagate through the material as a single wave. The

velocity of the elastic wave, C_e, is determined by substituting the equation for the normal stress into a combination of the conservation of mass and momentum equations given in eqns. (2.4) and (2.6), where $\sigma_n = P$ and $P_0 = 0$. The resultant

$$C_e = \left(\frac{\lambda + 2G}{\rho_0}\right)^{1/2} = \left(\frac{K + \frac{4}{3}G}{\rho_0}\right)^{1/2} = \left(\frac{E}{\rho_o}\right)^{1/2}, \qquad (2.19)$$

is the equation for longitudinal elastic waves in an unbounded medium. At point B, the material yields and plastically deforms along the solid curve from B to C.

Experimental data have shown that the bulk modulus, K, slowly increases with pressure. At point B, the discontinuous decrease in slope violates the condition for shock stability. As a result, the shock breaks up into two waves, an elastic and a plastic wave. The elastic wave propagates with a stress of σ_y moving with a velocity of C_e, followed by the plastic wave moving with a velocity C_{pl},

$$C_{pl} = \left(\frac{d\sigma/d\varepsilon}{\rho_o}\right)^{1/2}. \qquad (2.20)$$

At point C, the Rayleigh line for the plastic shock is an extension of the elastic line from point A to B and the velocity of the plastic wave is equal to or greater than the elastic wave. At this point the shock is stable and the stress wave travels through the material as a single wave. Shocks of this magnitude are described as strong shocks or overdriven shocks. Notice that at point B in Figure 2.5, the difference between the hydrostatic compression curve and the one-dimensional compression curve is 2/3 Y, which is also shown in eqn. (2.18). As the pressure and normal stress increases, the difference between the two curves becomes negligible. Therefore, at very high shock

pressures, the stress system can be regarded as hydrostatic thus justifying the simplified approach of hydrocodes.

Figure 2.6 shows a graphical representation summarizing the resulting stress waves, which can propagate through a material, in relation to the Hugoniot curve and Rayleigh line. At a shock pressure equal to P_1, a single elastic stress wave propagates through the material. At a higher pressure of P_2, the stress wave is unstable and breaks up into two waves. This results in an elastic stress wave followed by a plastic stress wave. In general, a stable wave can not exist unless the Hugoniot curve is steeper than the Rayleigh line at the final state. At an even higher pressure of P_3, the velocity of the plastic wave overtakes the elastic wave and a single stress wave propagates through the material.
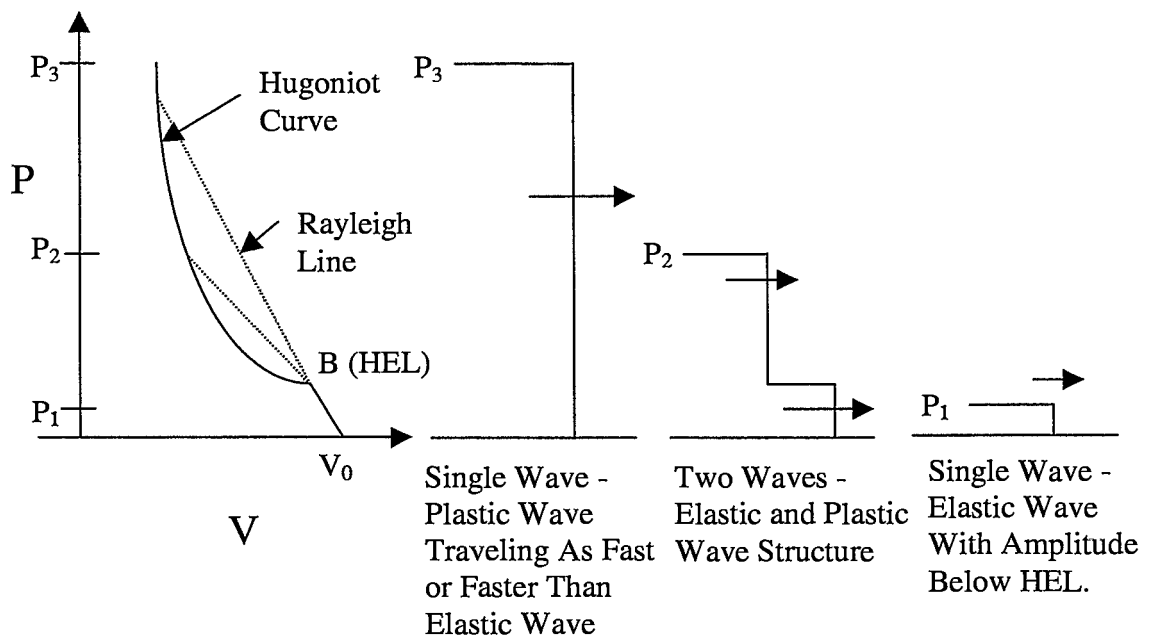
Figure 2.6: Wave Structure in Relation to the Hugoniot Curve and Rayleigh Line

A table with the mechanical properties and the velocity of elastic waves for five different materials is given in Table 2.2.

Table 2.2: Longitudinal Velocity of Elastic Waves

Material	Density (kg/m^{3})	G (GPa)	K (GPa)	Elastic Velocity (m/s)
Iron	7,850	81.6	170.1	5,960
Copper	8,930	48.3	137.8	4,760
Aluminum	2,700	26.1	75.6	6,400
Alumina	3,900	140.4	304.2	11,230
Uranium	18,950	66.1	143.26	3,490

Any time a material experiences high pressure loading, which may result from a shock wave, the effects of the pressure can be described with the use of the EOS for the material. If the state behind the shock wave is in equilibrium, then both the Rankine-Hugoniot and EOS relations must be satisfied. A common experimental form for the EOS is know as the $U_s - U_p$ form which can be expressed as

$$U_s = C_o + S_e U_p,$$
(2.21)

where C_o, is the isentropic sound speed and S_e is the slope of the $U_s - U_p$ curve.

In the study of shock waves, there are several different types of EOS equations. The Mie-Grüneisen EOS is common form used in numerical codes, which relates a state of pressure, volume, and energy to the state energy and pressure at a reference state. This reference state could, for example, be a point on the Hugoniot at the same volume (Meyers, 1994). In this case, the Mie-Grüneisen EOS can be written as,

$$P = P_H + \frac{\gamma}{V}(E - E_H),$$
(2.22)

where P_H is the Hugoniot pressure and E_H is the specific internal energy along the

Hugoniot line on the P-V plane. The Grüneisen constant, γ , can then be expressed as

$$\gamma = V \left(\frac{\partial P}{\partial E} \right)_V \qquad (2.23)$$

The shock and thermodynamic properties for different materials is given in Table 2.3

(Meyers, 1994), where C_p is the constant pressure specific heat.

Table 2.3: Shock and Thermodynamic Properties of Metals

Material	ρ_0 (kg/cm^3)	C_0 (mm/μs)	S_e	C_p (J/g-K)	γ
Be	1.85	8.00	1.12	0.18	1.2
Cu	8.93	3.94	1.49	0.40	2.0
Fe	7.85	3.57	1.92	0.45	1.8
Ni	8.87	4.60	1.44	0.44	2.0
Pb	11.35	2.05	1.46	0.13	2.8
U	18.95	2.49	2.20	0.12	2.1
W	19.22	4.03	1.24	0.13	1.8

At this point, a detailed explanation of the relationship between shock waves and

stress waves has been provided. The loading in this dissertation is not considered in the

range of a strong shock and once a shock propagates through a material, numerous waves

are released and developed (Ferm, 1998). In the absence of strong shocks, it is quite

common to see the terminology of shock waves and stress waves used interchangeably in

the literature depending on the author, the audience, and the loading conditions.

The previous explanation included an introduction to the Hugoniot curve,

Rayleigh Line, and equation of state. These principles will now be used to formulate the

equations representing the effects of the high pressure shock on the bulk modulus and

temperature in the material. The formulation for this part of the constitutive model closely follows the work of Johnson (1981) and Wallace (1980b).

Recall that the isentropic bulk modulus, K, is defined as

$$K = \left(\frac{\partial P}{\partial \varepsilon_v} \right)_s,$$

(2.24)

where ε_v is the volumetric strain and P is the pressure. Under shock loading, the pressure in the material can be found from the Hugoniot curve. Therefore, the modified bulk modulus is found by taking the partial derivative of the Hugoniot pressure with respect to the volumetric strain.

The formulation to find the Hugoniot pressure as a function of the volumetric strain begins with the conservation of momentum equation given in eqn. (2.6),

$$P - P_o = \rho_o U_s U_p.$$

(2.25)

The pressure on the Hugoniot, P_H is then found by applying the $U_s - U_p$ form of the EOS (eqn. (2-21)) to eqn. (2.25) with $P_o = 0$,

$$P_H = \rho_o U_p \left(C_o + S_e U_p \right).$$

(2.26)

Recall from eqn (2.4), the conservation of mass may be written as,

$$\rho_o U_s = \rho \left(U_s - U_p \right).$$

(2.27)

Substituting the $U_s - U_p$ form of the EOS into eqn. (2.27) gives,

$$U_p \left[1 + S_e \left(\frac{\rho_o}{\rho} - 1 \right) \right] = C_o \left[1 - \frac{\rho_o}{\rho} \right].$$

(2.28)

Recall, the volumetric strain, ε_v, is defined as the trace of the stress tensor or,

$$\varepsilon_v = 1 - \frac{V}{V_o} = 1 - \frac{\rho_o}{\rho} = (-1)\, \varepsilon_{ii}.$$

(2.29)

Substituting eqn. (2.29) into (2.28) and simplifying gives an equation for the particle velocity as a function of volumetric strain.

$$U_p = \frac{C_o \varepsilon_v}{1 - S_e \varepsilon_v} \tag{2.30}$$

Substituting eqn. (2.30) into eqn. (2.26) gives the following equation representing the Hugoniot pressure as a function of the volumetric strain.

$$P_H = \frac{\rho_o C_o^2 \varepsilon_v}{(1 - S_e \varepsilon_v)^2} \tag{2.31}$$

The partial derivative is then

$$\frac{\partial P_H}{\partial \varepsilon_v} = \frac{\rho_o C_o^2 (1 + S_e \varepsilon_v)}{(1 - S_e \varepsilon_v)^3}. \tag{2.32}$$

Therefore the factor by which the bulk modulus is modified from the high pressure shock is simply

$$\frac{(1 + S_e \varepsilon_v)}{(1 - S_e \varepsilon_v)^3}. \tag{2.33}$$

Next, a thermodynamic equation will be formulated to determine the change in temperature in the material as a result of plastic work and the high pressure shock. This formulation begins with the first law of thermodynamics for a closed system,

$$\delta Q - \delta W = dE, \tag{2.34}$$

where the work is defined as

$$\delta W = P \, dV \tag{2.35}$$

and the heat flux is defined as

$$\delta Q = T \, dS. \tag{2.36}$$

Substituting eqns. (2.35) and (2.36) into eqn. (2.34) yields

$$dE = T\ dS - P\ dV\ .$$ (2.37)

Recall, entropy S, is a function of temperature and volume and therefore

$$dS = \left(\frac{\partial S}{\partial T}\right)_V dT + \left(\frac{\partial S}{\partial V}\right)_T dV\ .$$ (2.38)

Multiplying the eqn. (2.38) by the temperature, T, gives

$$T\ dS = T\left(\frac{\partial S}{\partial T}\right)_V dT + T\left(\frac{\partial S}{\partial V}\right)_T dV\ .$$ (2.39)

The specific heat at constant volume is defined as

$$C_V = \left(\frac{\partial E}{\partial T}\right)_V = T\left(\frac{\partial S}{\partial T}\right)_V\ ,$$ (2.40)

which when substituted into eqn. (2.37) above gives

$$T\ dS = C_V\ dT + T\left(\frac{\partial S}{\partial V}\right)_V dV\ .$$ (2.41)

Using the following form of Maxwell's Equations,

$$\left(\frac{\partial S}{\partial V}\right)_T = \left(\frac{\partial P}{\partial T}\right)_V\ ,$$ (2.42)

eqn. (2.41) can be written as

$$T\ dS = C_V\ dT + T\left(\frac{\partial P}{\partial T}\right)_V dV\ ,$$ (2.43)

or

$$T\ dS = C_V\ dT + T\left(\frac{\partial P}{\partial E}\right)_V \left(\frac{\partial E}{\partial T}\right)_V dV\ .$$ (2.44)

Substituting eqns. (2.22) and (2.23) from the Hugoniot and Grüneisen relations into

35

eqn (2.44) gives

$$T \, dS = C_V \, dT - T \, \gamma \left(\frac{\partial E}{\partial T} \right)_V d\varepsilon_v,$$

(2.45)

or

$$T \, dS = C_V \, dT - T \, \gamma \, C_V \, d\varepsilon_v.$$

(2.46)

Solving for dT gives,

$$dT = T \, \gamma \, d\varepsilon_v + \frac{T \, dS}{C_v}$$

(2.47)

For adiabatic solids, $\dot{Q} = 0$, and as a result

$$dW^{pl} = T \, dS = \frac{\sigma_{ij} \, d\varepsilon_{ij}^{pl}}{\rho}$$

(2.48)

Substituting eqn. (2.48) into (2.47) gives the equation for calculating the temperature rise

in the material due to the high pressure shock and plastic work.

$$dT = T \, \gamma \, d\varepsilon_v + \frac{\sigma_{ij} \, d\varepsilon_{ij}^{pl}}{C_V \rho}$$

(2.49)

The increase in temperature as a result of the shock loading and the plastic work is given

by the first and second respective terms on the right side of eqn. (2.49). The term that

accounts for the shock heating, along with eqn. (2.33) which represents the change in the

bulk modulus, are determined in the EOS subroutine of the constitutive model. These

values are then passed back to the constitutive model to be used in the Gurson subroutine.

The details of their implementation into the constitutive model will be discussed in the

next chapter.

2.3 Microvoid Damage Model

The rate dependent plastic deformation that occurs during radial expansion of a ductile cylindrical shell causes material bonds to be broken which nucleates voids in the previously intact material. These voids are thought to nucleate predominantly at secondary phase particles in the material because of their stress raising effect or low bond strength with the surrounding material during plastic deformation (Shockey et al. 1980). Voids can also nucleate prior to, or as a result of, instabilities in the material. The voids continue to grow by means of local plastic flow or diffusion and coalescence with neighboring voids. It is therefore important to understand and account for void nucleation and void kinetics in the failure of ductile materials.

Fracture by the growth of microvoids in materials was observed by Tipper (1949) in 1949 and later by Puttick (1959) and Rogers (1960). Early work on the growth of voids and microstructural damage in the plastic region of behavior for ductile materials under combined loading was performed in the late 1960's (McClintock, 1968; Rice and Tracey 1969). Rice and Tracey derive a growth law for a spherical void that depends on both the plastic strain and the mean tensile stress. They considered only a single void in an infinite medium and thus void growth does not affect the imposed stress field. Later Gurson (1977), extended their model to consider a finite block of material with a continuum approach. Gurson's model depends on the plastic strain and mean tensile stress and demonstrates the effects of the voids on the surrounding stress field. By assuming the material behaves as a continuum, voids appear in the model indirectly and their effects are averaged through the material.

In addition to the strain, entropy, and temperature in the constitutive relations, functions for the distribution, orientation, and size of the microvoids are introduced to describe the current state of the material. This MSFM type of constitutive approach is justified for two reasons. First, the specimen size is large in comparison to the size of the flaws. Secondly, the flaws are distributed throughout the material and are numerous enough that their behavior can be averaged like molecular collisions in a material.

Curran et al. (1987) categorize failure in polycrystalline solids by either ductile void growth or brittle crack extension. The bulk of existing literature assumes ductile void growth occurs by either diffusion or plastic flow from spherically symmetric tension or by a combination of symmetric tension and shear stress. Chadwick (1959) and Hopkins (1960) provided early results on the growth of voids subjected to spherically symmetric tension. Carrol and Holt (1972) continued this work and now much of the current literature considers only the effects of spherically symmetric tension, which is a simplification of the combined loading problem.

Gurson's model was observed to greatly over predict failure strains in real materials, which prompted Tvergaard (1981, 1982) to adjust Gurson's constitutive equations. His modification was to include an effective void volume fraction in the constitutive model. In addition, Tvergaard introduced several coefficients to account for void interaction effects. Needleman and Rice (1978) proposed a general equation to represent the nucleation rate of voids in the material. This rate is controlled by either the maximum normal stress or maximum plastic strain (Chu and Needleman,1980; Needleman, 1987; Tvergaard, 1987).

The Gurson model is more comprehensive and computationally intensive than the model proposed by Carrol and Holt. However, it appears to be more commonly used in the recent literature. The modifications by Tvergaard and Needleman have greatly improved the model and in recent literature, this model has been referred to as the Gurson-Tvergaard-Needleman (GTN) model. Its numerical implementation is a major part of this dissertation.

The yield condition for the GTN model can be expressed as:

$$\phi = \left(\frac{\sigma}{\sigma_f}\right)^2 + 2q_1 f^* \cosh\left(-\frac{3q_2 P}{2\sigma_f}\right) - \left(1 + q_3 f^{*2}\right) = 0 \qquad (2.50)$$

where

$$\sigma = \sqrt{\frac{3}{2} S_{ij} S_{ij}} \qquad (2.51)$$

is the effective Mises stress,

$$S_{ij} = \sigma_{ij} - \frac{1}{3}\sigma_{ij}\delta_{ij} \qquad (2.52)$$

is the deviatoric stress,

$$P = -\frac{1}{3}\sigma_{ii} \qquad (2.53)$$

is the hydrostatic pressure and σ_f is the flow stress. The original model derived by Gurson was formulated for a perfectly plastic material with spherically symmetric deformations around a single void. This model can be recovered by setting $q_1 = q_2 = q_3 = 1$ in eqn (2.50). The variables q_1, q_2, and q_3 are the material parameters introduced by Tvergaard (1981, 1982). Tvergaard's modifications considerably improved the model by demonstrating closer agreement with experimental data. The

GTN model is usually applied to ductile materials like OFE copper and aluminum. Typical values for q_1, q_2, and q_3 are $q_1 = 1.0\text{-}1.5$, $q_2 = 1.0$, and $q_3 = q_1^2 = 1.0 - 2.25$.

The void volume fraction, f, is defined as a function of the relative density, ζ, of the material. The relative density, ζ, is defined as the ratio of the volume of solid material to the total volume of material. The void volume fraction and relative density are related by

$$f = 1 - \zeta = 1 - \frac{\rho_s}{\rho_o}. \tag{2.54}$$

The material is assumed to be fully dense if $f = 0$ ($\zeta = 1$), and in this case the Gurson yield surface reduces to the Von-Mises model. In the case of $f = 1$ ($\zeta = 0$), the material is assumed to be fully voided (100% voids) and the material has lost its stress carrying capacity.

The parameter f^*, which was introduced by Needleman and Tvergaard (1984), is the modified damage parameter that accounts for void coalescence. This parameter is a function of the void volume fraction f and is defined as

$$f^* = \begin{cases} f & \text{if } f \leq f_c \\ f_c + \dfrac{\bar{f}_F - f_c}{f_F - f_c}(f - f_c) & \text{if } f_c < f < f_F \\ \bar{f}_F & \text{if } f \geq f_F \end{cases} \tag{2.55}$$

where f_c is the critical value of the void volume fraction and f_F is the final value of void volume fraction at which the material has completely lost its stress carrying capacity. The function for $\bar{f}_F$ is defined as

$$\bar{f}_F = \frac{q_1 + \sqrt{q_1^2 - q_3}}{q_3} \qquad (2.56)$$

The total increment in the void volume fraction is the sum of the increment due to void growth and the increment due to void nucleation, or

$$df = df_{gr} + df_{nucl}. \qquad (2.57)$$

The growth of existing voids is based on the conservation of mass and is expressed as

$$df_{gr} = (1 - f) d\varepsilon_{ii}^{pl}, \qquad (2.58)$$

where $d\varepsilon_{ii}^{pl}$ is the trace of the plastic strain tensor. The nucleation of voids occurs by decohesion of the interface between second phase particles and the matrix, by particle fracture, or from broken material bonds. The nucleation model suggested in the current literature can include strain or stress based nucleation. At this time, the work in this dissertation considers only strain based nucleation. The strain based nucleation rate is expressed as,

$$df_{nucl} = A \, d\bar{\varepsilon}_m^{pl}, \qquad (2.59)$$

where

$$A = \frac{f_N}{s_N \sqrt{2\pi}} \exp\left[-\frac{1}{2} \left(\frac{\bar{\varepsilon}_m^{pl} - \varepsilon_N}{s_N} \right)^2 \right], \qquad (2.60)$$

and the mean plastic strain, $d\bar{\varepsilon}_m^{pl}$, is found from,

$$(1 - f)\sigma_f \, d\bar{\varepsilon}_m^{pl} = \sigma_{ij} \, d\varepsilon_{ij}^{pl}. \qquad (2.61)$$

In eqn. (2.60), f_N is the volume fraction for nucleating particles, ε_N is the main strain for nucleation, and s_N is the corresponding standard deviation. Recent literature

(ABAQUS, 1997) suggests the following range of values for typical metals: $f_N = 0.04$, $s_N = 0.05 - 0.1$, $\varepsilon_N = 0.1 - 0.3$.

Several of the equations presented in this chapter will reappear in the next chapter as the implementation of the constitutive model is discussed. The method used to determine the increment in plastic strain is also discussed in Chapter 3. In short, an increment in total strain is passed to the constitutive model. The constitutive model then iterates to determine the elastic strains and stresses to remain on the yield surface and not violate the yield condition presented in eqn (2.50). The iteration technique, which is occasionally called the cutting plane algorithm, is discussed in Chapter 3. In addition, Chapter 3 discusses other aspects of the constitutive model such as the optional "element remove" subroutine, which may be used to prevent elements from inverting and stopping the computation by removing them from the calculation.

3.0 Numerical Model

This chapter describes the implementation of the constitutive model into the ABAQUS (1997) code through what ABAQUS calls a VUMAT subroutine. The constitutive model for this analysis is divided into four basic modules: shock effects, GTN plasticity, void growth and strength (Johnson-Cook). In general, the VUMAT subroutine is used to define the mechanical constitutive behavior of the material and if necessary update or use solution dependent state variables to track the material response.

Finite element codes such as ABAQUS Explicit are widely used in industry and at government laboratories such as Los Alamos National Laboratory. These codes are capable of analyzing highly non-linear structural dynamics problems. ABAQUS is a commercially available Lagrangian finite element package. It offers post processing capabilities and a significant amount of user flexibility. Johnson (1981) demonstrated the implementation of his constitutive model using a finite difference approach. However, since numerical codes exist at Los Alamos National Laboratory to preprocess and post process finite element results from ABAQUS along with a strong experience base, ABAQUS was chosen for the numerical code. Enhancement of ABAQUS with additional code development in the form of a VUMAT subroutine will expedite the implementation of new constitutive models and provide a platform to analyze complex geometries.

During the solution process, ABAQUS calculates an increment in strain based on the boundary conditions (such as an increment in load) and the previous state of stress.

This increment in strain is passed to the VUMAT subroutine. The subroutine then returns the state of stress for the material. A large number of parameters can be passed into the VUMAT subroutine. Most of these parameters are either user defined material properties or solution variables, which provide information regarding the last state of the solution and the increment in strain. The user definable variables include the updated stress tensor, state variables, internal energy, and inelastic energy.

The VUMAT subroutine developed for this dissertation consists of a main subroutine and five other smaller subroutines: an equation of state (EOS) subroutine, a GTN subroutine, a Johnson-Cook subroutine, a void growth subroutine, and an element remove subroutine. The EOS and element remove subroutines are optional and can be activated by the user. This allows the code to skip those calculations.

Initially, the main VUMAT subroutine is called. Then if activated, the main subroutine calls the EOS subroutine to modify the bulk modulus and determine the shock heating effects. These results are then returned to the main VUMAT subroutine. Next the main subroutine calls the GTN subroutine. The GTN subroutine calculates the necessary parameters for the strength model and then calls the Johnson-Cook subroutine to determine the flow stress. This flow stress is returned back to the GTN subroutine where the code iterates to converge to a point on the yield surface. At this point, the stresses, energies, and temperatures are updated and passed back to the main subroutine. Next the main VUMAT subroutine calls the void subroutine. The void subroutine determines the nucleation and growth rate for the voids and passes back the new volumetric void concentration in the material. Finally, at the user's discretion, the code enters the element remove subroutine. This subroutine eliminates elements from the

computation based on user specified parameters like volumetric void concentrations or equivalent plastic strain. A flow chart of the VUMAT subroutine is shown in Figure 3.1. It is important to understand that once the code enters the VUMAT subroutine, which is indicated by the dotted oval in Figure 3.1, it does not return to ABAQUS until the stresses and state variables are updated. The circled numbers in Figure 3.1 indicate the calling order for each subroutine. The entire VUMAT subroutine consists of approximately 2300 lines of commented Fortran source code. The implementation of the constitutive model into the VUMAT subroutine is explained in more detail in the remaining sections of this chapter.
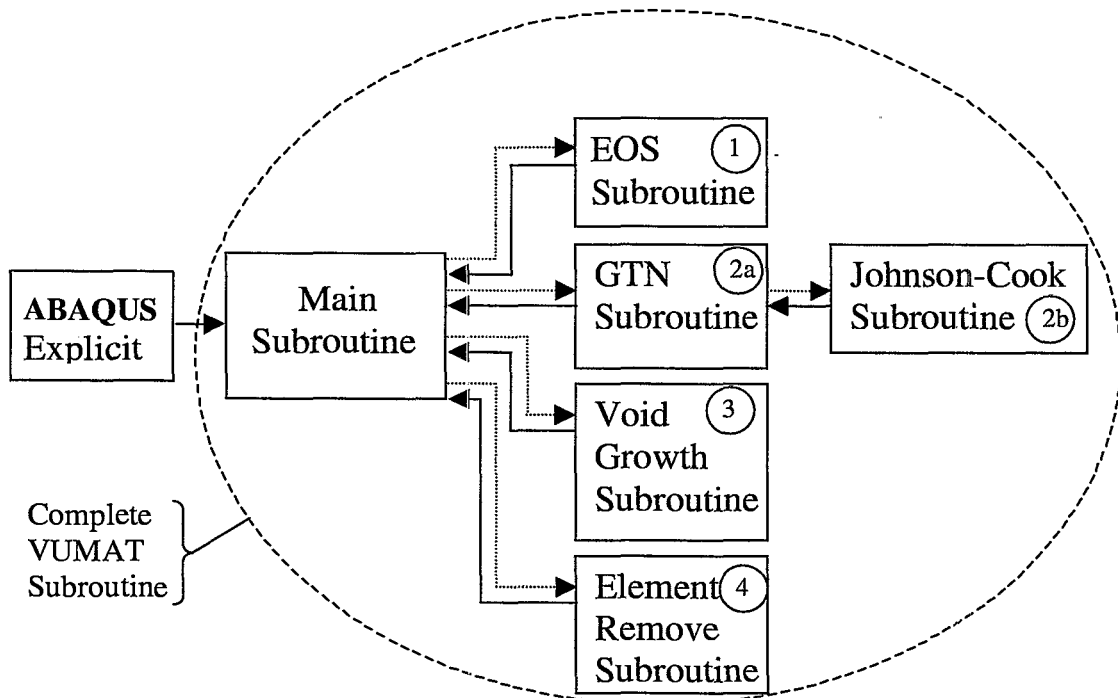
Figure 3.1 Flow Chart for VUMAT Subroutine

3.1 EOS Subroutine

As mentioned earlier, the first subroutine called from the main VUMAT subroutine is the equation of state subroutine. This subroutine determines the

temperature change and the modified bulk modulus resulting from the high pressure shock. Recall that the increment in strain is passed into this subroutine and as a result, this subroutine begins by calculating the volumetric strain increment, where compression is defined as being positive in this subroutine,

$$d\varepsilon_v = (-1.0)\, d\varepsilon_{ii}.$$ (3.1)

This increment is then added to the total volumetric strain at previous increment,

$$\varepsilon_v = \varepsilon_v^{old} + d\varepsilon_v$$ (3.2)

Recall from Chapter 2, the particle velocity, shock velocity, and Hugoniot pressure are calculated with

$$U_p = \frac{C_o \varepsilon_v}{1 - S_e \varepsilon_v}$$ (3.3)

$$U_s = C_o + S_e U_p$$ (3.4)

$$P_H = \frac{\rho_o C_o^2 \varepsilon_v}{(1 - S_e \varepsilon_v)^2}$$ (3.5)

The shock velocity is not specifically needed for the constitutive model. However, its value is stored as a solution dependent variable. If the particle velocity is positive, then the bulk modulus and material temperatures are modified based on the volumetric strain. For positive particle velocities $(U_p > 0)$, the new bulk modulus, K_{new}, and shock temperature, T_s, are found using

$$K_{new} = K_o \frac{(1.0 + S_e \varepsilon_v)}{(1.0 - S_e \varepsilon_v)^3},$$ (3.6)

$$T_s = T_o \gamma \varepsilon_v,$$ (3.7)

otherwise, the default bulk modulus, K_o, remains unchanged and the shock temperature is set to zero,

$$K_{new} = K_o \qquad (3.8)$$

$$T_s = 0.0. \qquad (3.9)$$

At this point, the solution dependent variables are updated and the computation returns to the main VUMAT subroutine. The next subroutine called updates the stresses based on the yield surface calculations defined by the GTN model.

3.2 GTN Subroutine

As mentioned in Chapter 2, the form of the GTN model implemented in this dissertation is a combination of the work completed by Gurson, Tvergaard and Needleman. This model has been implemented into other numerical codes like ABAQUS/Standard (Hao & Brocks, 1997) and NIKE (Engelmann & Whirley, 1992).

An iterative technique must be used to obtain the stresses and not violate the yield conditions. The technique adopted for this dissertation is called the cutting-plane algorithm and is described by Ortiz and Popov (1985) and Ortiz and Simo (1986). This algorithm is based on linearization of the plastic consistency condition for the current iteration and satisfaction of the plastic consistency for the new iteration. The cutting plane algorithm is very efficient and demonstrates reasonable accuracy (Ortiz and Simo, 1986). However, it is necessary to take the derivative of the yield function, which is not always straightforward.

The first operation this subroutine performs is to reformulate the elastic constant matrix, zero temporary variables, and set the convergence tolerance. Recall the EOS

subroutine may have modified the bulk modulus. The updated elastic constant matrix, D_{ij}, becomes,

$$D_{ij} = \begin{bmatrix} \left(K_{new} - \frac{2}{3}G\right) + 2G & \left(K_{new} - \frac{2}{3}G\right) & \left(K_{new} - \frac{2}{3}G\right) & 0 & 0 & 0 \\ \left(K_{new} - \frac{2}{3}G\right) & \left(K_{new} - \frac{2}{3}G\right) + 2G & \left(K_{new} - \frac{2}{3}G\right) & 0 & 0 & 0 \\ \left(K_{new} - \frac{2}{3}G\right) & \left(K_{new} - \frac{2}{3}G\right) & \left(K_{new} - \frac{2}{3}G\right) + 2G & 0 & 0 & 0 \\ 0 & 0 & 0 & G & 0 & 0 \\ 0 & 0 & 0 & 0 & G & 0 \\ 0 & 0 & 0 & 0 & 0 & G \end{bmatrix} \qquad (3.10)$$

Next, the subroutine performs a few preliminary calculations, which are required to determine the flow stress in the Johnson-Cook subroutine. The increment in plastic strain is found from

$$d\varepsilon_{ij}^{pl} = d\varepsilon_{ij} - \frac{1}{3}d\varepsilon_{kk}\delta_{ij}, \qquad (3.11)$$

where $d\varepsilon_{ij}$ is the strain increment and $d\varepsilon_{ij}^{pl}$ is the plastic strain increment. The incremental equivalent plastic strain is found from,

$$d\varepsilon^{pl} = \sqrt{\frac{2}{3}d\varepsilon_{ij}^{pl}\,d\varepsilon_{ij}^{pl}}\,, \qquad (3.12)$$

and the equivalent plastic strain rate is calculated using,

$$\dot{\varepsilon}^{pl} = \frac{d\varepsilon^{pl}}{dt}, \qquad (3.13)$$

where dt is the current time step. The equivalent plastic strain rate and the total plastic strain are passed to the Johnson-Cook subroutine along with the current material temperature. The Johnson-Cook subroutine, which is discussed in the next section, returns the flow stress.

The iteration begins with the computation of the plastic strain increment,

$$d\varepsilon_{ij}^{pl} = d\varepsilon_{ij}^{pl} + \Delta\lambda \, D_{ij}\psi_i . \qquad (3.14)$$

Initially, $\Delta\lambda$ and $d\varepsilon_{ij}^{pl}$ are zero, so the plastic strain increment is also zero. The equivalent plastic strain increment is recalculated in the iteration loop using,

$$d\varepsilon^{pl} = \sqrt{\frac{2}{3} d\varepsilon_{ij}^{pl} d\varepsilon_{ij}^{pl}} \qquad (3.15)$$

Next the total elastic strain is calculated using,

$$\varepsilon_{ij}^{el} = \varepsilon_{ij}^{el_{old}} + \left(d\varepsilon_{ij} - d\varepsilon_{ij}^{pl}\right), \qquad (3.16)$$

where $\varepsilon_{ij}^{el_{old}}$ is the total elastic strain at the previous converged increment and $d\varepsilon_{ij}^{pl}$, is found from eqn. (3.14). At this point the new trial stresses are computed,

$$\sigma_{ij}^{tr} = D_{ik} \, \varepsilon_{kj}^{el} . \qquad (3.17)$$

For compressive shock loading, the hyperbolic cosine part of the yield function given in eqn. (2.50) becomes unstable at large hydrostatic pressures. As a result, a pressure cutoff was implemented to modify q_2 and stabilize the yield function. The concept of a pressure cutoff is unique to this dissertation and is based on the assumption that the GTN yield surface is not applicable to materials subjected to high hydrostatic compression. A cut-off pressure, which is set as a user supplied parameter, will ensure stability and not affect the resultant stresses. If the trace of the stress tensor is more compressive than allowed by the user defined cut-off pressure, then,

$$q_2^{new} = abs\left(\frac{\sigma_f}{\sigma_{ii}}\right), \qquad (3.18)$$

otherwise, q_2, remains unchanged and the yield function is evaluated. Recall the yield function (see eqn. 2.50) is defined as

49

$$\phi = \left(\frac{\sigma}{\sigma_f}\right)^2 + 2q_1 f^* \cosh\left(-\frac{3q_2 P}{2\sigma_f}\right) - \left(1 + q_3 f^{*2}\right) = 0. \tag{3.19}$$

If the yield function is less than or equal to zero, then the trial stresses become the new stresses. Otherwise, the yield surface is extended and the iteration loop continues until it determines the elastic-plastic solution.

If an elastic-plastic solution exists, the iteration loop calculates the change in the plastic consistency parameter, $\Delta\lambda$. This new $\Delta\lambda$, is then used to recalculate the plastic strains in eqn. (3.14). Based on the new plastic strains, the elastic strains given by eqn. (3.16) are updated and the new trial stresses are found using eqn. (3.17). These trial stresses are then used to reevaluate the yield function, eqn. (3.19), and convergence is checked. If the yield function is still not less than or equal to zero, the iteration continues.

The formulation for calculating change in the plastic consistency parameter closely follows reports by Engelmann and Whirley (1992) and Ortiz and Simo (1986), and is briefly summarized here. First let ψ_i be a vector of the equivalent plastic strain and void volume fraction,

$$\psi_i = \left\{ \begin{matrix} \varepsilon^{pl} \\ f \end{matrix} \right\}, \tag{3.20}$$

and let the vector function $h_i(\sigma, \psi)$ be defined such that,

$$\Delta\psi_i(\sigma, \psi) = \Delta\lambda\, h_i(\sigma, \psi). \tag{3.21}$$

Next, define a vector function $\xi_i(\sigma, \psi)$ as the gradient of the yield function with respect to the history variables,

$$\xi_i(\sigma, \psi) = \frac{\partial\phi}{\partial\psi_i}(\sigma, \psi). \tag{3.22}$$

In addition, define a second order tensor $v_{ij}(\sigma,\psi)$ as the gradient of the yield function with respect to stress,

$$v_{ij}(\sigma,\psi) = \frac{\partial\phi}{\partial\sigma_{ij}}(\sigma,\psi). \tag{3.23}$$

The change in the plastic consistency parameter is then

$$\Delta\lambda = \frac{\phi}{v_{ij}D_{jk}v_{ik} - \xi_l h_l}, \tag{3.24}$$

where, ϕ, is the yield function. The specific definitions of ξ_l, v_{ik}, and h_l in terms of the stress components are:

$$\xi_1 = \frac{\partial\phi}{\partial\varepsilon_{ij}^{pl}} = -\frac{2H}{\sigma_f^3}\left[\frac{2}{3}\sigma_{ij}\sigma_{ij} - \frac{1}{2}\sigma_{kk}\sigma_{ll}\right] - \frac{H f^* q_1 \sigma_{kk}}{\sigma_f^2}\sinh\left(\frac{q_2\,\sigma_{kk}}{2\sigma_f}\right), \tag{3.25}$$

$$\xi_2 = \frac{\partial\phi}{\partial f} = 2q_1\cosh\left(\frac{q_2\,\sigma_{kk}}{2\sigma_f}\right) - 2q_2 f^*, \tag{3.26}$$

$$v_{ik} = \frac{\partial\phi}{\partial\sigma_{ik}} = \frac{1}{\sigma_f^2}[3\sigma_{ik} - \sigma_{ll}\delta_{ik}] + \frac{f^* q_1}{\sigma_f}\sinh\left(\frac{q_2\,\sigma_{ll}}{2\sigma_f}\right)\delta_{ik}, \tag{3.27}$$

$$h_1 = \sqrt{\frac{2}{3}v_{ij}v_{ij}}, \tag{3.28}$$

$$h_2 = (1-f)v_{ii}, \tag{3.29}$$

where H is the tangent of the flow surface. The tangent of the flow stress equation given by Johnson and Cook is calculated as

$$H = \frac{(\sigma_f - \sigma_f^{old})}{d\varepsilon^{pl}}. \tag{3.30}$$

At this point, the iteration is complete and the elastic-plastic solution is known. Next the total plastic strain is updated with the new increments in plastic strain. The increment in plastic work is also calculated as,

$$dW^{pl} = \frac{\sigma_{ij} \, d\varepsilon_{ij}^{pl}}{\rho}.$$

(3.31)

Notice eqn. (3.31) is not written in terms of the deviatoric stress tensor but rather the total stress tensor. This is a result of incorporating microvoids, which makes the contribution of the spherical stress tensor important in the calculation of the plastic work. The increment in internal energy is simply,

$$dE = \frac{1}{2} \frac{\sigma_{ij} \, d\varepsilon_{ij}}{\rho}.$$

(3.32)

The total plastic work and total internal energy, whose units are for example J/kg, are then found by adding the respective increments from eqns. (3.31) and (3.32) to the values at the previously converged increment.

The new temperature of the material is calculated using both the temperature rise as a result of the shock heating and the temperature resulting from the plastic work.

$$T^{new} = T^{int} + T_s + \frac{\sum dW^{pl}}{C_v},$$

(3.33)

where T^{init} is the initial temperature, $\sum dW^{pl}$ is the total increment in plastic work, and C_v is the specific heat. Recall that the shock temperature is passed into this subroutine from the EOS subroutine. Finally, the mean plastic strain is calculated from the increment in plastic work, the current void volume fraction, and the flow stress. This value, which is expressed as,

$$d\bar{\varepsilon}_m^{pl} = \frac{\sigma_{ij}\, d\varepsilon_{ij}^{pl}}{(1-f)\sigma_f}, \qquad\qquad (3.34)$$

is needed to calculate the void nucleation rate in the void subroutine and is also shown as eqn. (2.61) in Chapter 2.

At the end of this subroutine, several variables are saved as solution dependent variables. Any variable saved as a solution dependent variable can be used in subsequent subroutines or during the next time step and the user can always plot the time history response of solution dependent variables during post processing.

3.3 Strength Subroutine

As mentioned in Chapter 2 and the previous section, the flow stress is based on the Johnson-Cook strength model and is calculated using the current plastic strain, strain-rate, and temperature. From eqn. (2.1), the equation for the flow stress is written as,

$$\sigma_f = \left(A + B\varepsilon^n\right)\left(1 + C\ln\dot{\varepsilon}^*\right)\left(1 - T^{*m}\right) \qquad\qquad (3.35)$$

The five experimentally determined parameters (A, B, C, n, m) are supplied as constants to the VUMAT. The current plastic strain, strain-rate, and temperature are passed into this Johnson-Cook subroutine from the GTN subroutine. The Johnson-Cook subroutine then returns the allowable flow stress. By separating the flow stress calculations from the main body of the VUMAT, it is relatively easy to implement other strength models at a later time.

3.4 Void Subroutine

The implementation of the void model was separated from the GTN subroutine to allow the user to implement different constitutive laws involving other forms of void growth, nucleation, and coalescence. Recall from eqns (2.55) through (2.60) in Chapter 2, the rate of change in the void volume fraction can be written as,

$$df = df_{gr} + df_{nucl}, \tag{3.36}$$

where the growth rate is dependent on the trace of the plastic strain rate and the nucleation is based on the equivalent flow stress.

At the start of this subroutine, the first series of calculations set the constants that will be used in the subroutine. One of these constants is

$$\bar{f}_F = \frac{q_1 + \sqrt{q_1^2 - q_3}}{q_3} \tag{3.37}$$

which is the void volume fraction at which there is a complete loss of stress carrying capacity in the material. Next the increment in void growth,

$$df_{gr} = (1 - f) d\varepsilon_{ii}^{pl}, \tag{3.38}$$

is calculated using the trace of the increment in the plastic strain tensor from the GTN model. To determine the increment in nucleated voids, the parameter

$$A = \frac{f_N}{s_N \sqrt{2\pi}} \exp\left[-\frac{1}{2} \left(\frac{\bar{\varepsilon}_m^{pl} - \varepsilon_N}{s_N} \right)^2 \right], \tag{3.39}$$

is determined and applied to

$$df_{nucl} = A \, d\bar{\varepsilon}_m^{pl}, \tag{3.40}$$

using the mean plastic strain from the GTN model. Combining eqns. (3.38) and (3.40) into (3.36) gives the total increment in the void volume fraction. The increment in the

void volume fraction is added to the total volume fraction from the previous increment to obtain f. The new void volume fraction, f^*, which is passed back from this subroutine is defined from the following equation as explained in eqn (2.55) from Chapter 2.

$$f^* = \begin{cases} f & \text{if } f \leq f_c \\ f_c + \dfrac{\bar{f}_F - f_c}{f_F - f_c}(f - f_c) & \text{if } f_c < f < f_F \\ \bar{f}_F & \text{if } f \geq f_F \end{cases} \qquad (3.41)$$

If this is the first increment, this subroutine initializes the void volume fraction in the material with either a constant or random distribution of voids. A constant distribution of voids is defined with the user defined variable, f^{init}, using

$$f^* = f^{init}, \qquad (3.42)$$

and a random distribution of voids is defined using

$$f^* = f^{init} + 5.0 \, r \, f^{init}, \qquad (3.42)$$

where r is a randomly generated number from 0 to 1.0. For example, if f^{init} is 0.001, then the material will have a random distribution of voids ranging from 0.001-0.005.

3.5 "Element Remove" Subroutine

The element remove subroutine is simple and straightforward. ABAQUS allows the user to define a solution dependent variable that indicates the element is to be removed from the calculations. The corresponding stiffness of the targeted element is then significantly reduced to effectively remove this element from the calculations. The element does remain in the mesh, but does not interact any further with the surrounding elements. This allows the user to 'remove' elements based on a predetermined set of

specifications. For example, if the plastic strain or void volume fraction in the element reaches a selected critical value, the element is removed from the calculations. One negative aspect of this technique is that it does not allow for a gradual decrease in stiffness. However, this subroutine was written to allow the user to implement a stiffness degradation model at a later time. Currently, this subroutine removes elements based on either the accumulated equivalent plastic strain or void volume fraction.

3.6 HE Burn Model

The high explosive burn model used in this dissertation is developed and maintained by ABAQUS and is not part of the VUMAT developed in this dissertation. ABAQUS uses the Jones-Wilkens-Lee (JWL) equation of state to model the pressure generated by the release of chemical energy from the explosive. The reaction and initiation of the EOS is implemented using a program burn model. The program burn model determines the initiation time by a geometric construction using the detonation wave speed and the distance of the material points from the detonation point.

This model is simple to use and the parameters are widely available in the current literature. To activate this model, the user simply provides the detonation point(s) and the high explosive (HE) parameters for the JWL equation of state. The HE used throughout this dissertation is PBX-9501. This type HE was used because it is readily obtainable with a well documented EOS and it is easy to fabricate and machine to reasonable dimensional tolerances. The JWL parameters for PBX-9501 (Dobratz, 1981) are provided in Table 3.1, where C_d is the detonation wave speed, E_{mo} is the initial energy per unit mass, and P_{cj} is the cutoff pressure.

Table 3.1: JWL Parameters for PBX-9501

A (Pa)	B (Pa)	ω	R_1	R_2	C_d (m/s)	E_{mo} (J/kg)	P_{cj} (Pa)
8.545×10^{11}	2.049×10^{10}	0.25	4.6	1.35	8830.0	5.543×10^{6}	0.0

3.7 Preliminary Results

A small axisymmetric model was developed to demonstrate the capabilities of this constitutive model. This model consists of an axisymmetric ring of copper filled with high explosive. The mesh for this model is shown in Figure 3.2.
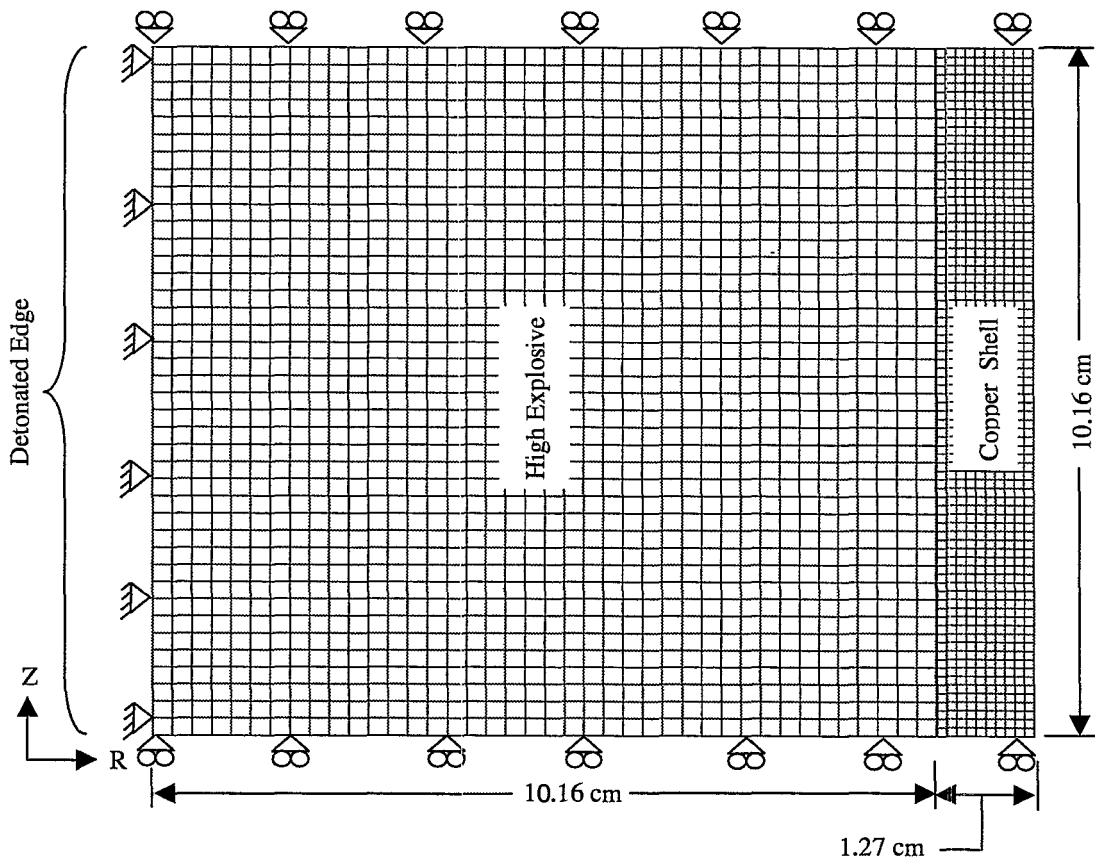
**Figure 3.2: Mesh for Preliminary Axisymmetric Ring Model**

The elements used in this model are four node, linear, axisymmetric elements. There are 1600 elements in the HE and 800 elements in the cylindrical shell. A 0.127 mm gap exists between the HE and the copper shell. A contact surface is prescribed between the HE and the shell. This contact surface allows the elements on the boundary to slide relative to one another without penetration. The effects of friction are not included in the model and thus only a normal force relative to the contact surface is transmitted across the HE-copper boundary. The HE is line detonated along the axis of symmetry (R = 0) to provide uniform radial expansion. A symmetry boundary condition is applied to the top and bottom of the mesh, as it appears in Figure 3.2. This allows the geometry to expand freely in the radial direction, away from the detonated axis, but with no displacement in the Z-direction, normal to the rollers. A table summarizing the user parameters supplied to the constitutive model is provided in Table 3.2.

Table 3.2: User Parameters Supplied to the Constitutive Model for the Copper Ring

Model	Description	Units	Value
Johnson-Cook Strength Model	Material Density	kg/m^3	8945.0
	Specific Heat	J/kg-K	383.5
	Initial Temperature	K	294.26
	Room Temperature	K	294.26
	Melt Temperature	K	1355.93
	Shear Modulus	Pa	4.63×10^{10}
	Yield Stress	Pa	8.963×10^{7}
	Hardening Coef.	Pa	2.916×10^{8}
	Hardening Exp.	-	0.31
	Strain-Rate Coef.	-	0.025
	Thermal Softening Exp.	-	1.09
	Pressure Hardening Term	Pa	0.0
	Strength Cut-off	Pa	6.895×10^{10}
	On/Off Flag (1-on, 0-off)	-	1.0
EOS Model	Bulk Modulus	Pa	1.372×10^{11}
	Sound Speed - C_0	m/s	3940.0
	Slope of U_s-U_p Curve - S	-	1.49
	Grüneisen Coef. - γ	-	1.96
	Tensile Pressure Cut-off	Pa	6.895×10^{10}
	On/Off Flag (1-on, 0-off)	-	1.0
GTN Void Model	q_1	-	1.5
	q_2	-	1.0
	q_3	-	2.25
	f_F	-	0.85
	f_c	-	0.85
	Init. Void Vol. Fract. - f^{init}	-	0.001
	E_n	-	0.3
	S_n	-	0.1
	F_n	-	0.04
	Void Nucleation On/Off	-	1.0
	Random Voids On/Off	-	1.0
	On/Off Flag (1-on, 0-off)	-	1.0
	Void Pressure Cut-off	Pa	-1.0×10^{6}

The effect of the shock on the bulk modulus is shown in Figure 3.3. This figure

shows plots of the user supplied bulk modulus and modified bulk modulus vs. time for an

element on the ID and OD of the cylinder. When the EOS is not activated, the user

supplied bulk modulus, given in Table 3.2, is used throughout the calculations and is

constant with time. Otherwise when the EOS is activated, the bulk modulus in the

material is modified to include the effects of the high pressure shock. Notice that the

shock effect on the bulk modulus is much less for an element on the outside of the

cylinder. This is a result of rarefraction waves, which diminish the magnitude of the

shock as it travels through the cylinder wall.
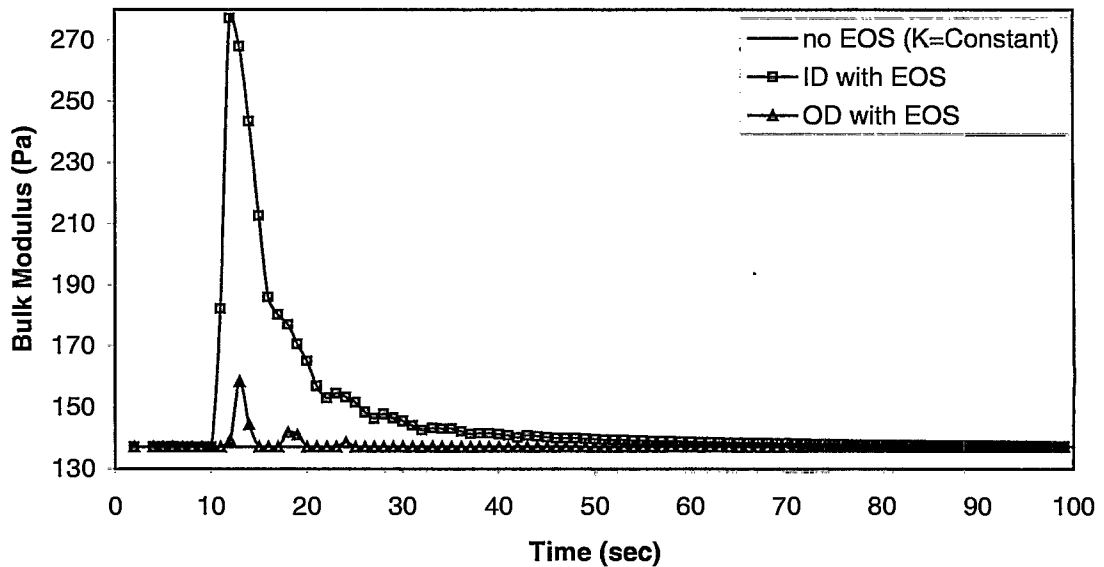

Figure 3.3: Shock EOS Effects on the Bulk Modulus

As expected, the temperature change resulting from the shock loading shows a

similar effect. A graph of the temperature change from the high pressure shock and

plastic deformation is shown in Figure 3.4. This figure shows the resulting temperature

vs. time for an element on the OD and ID with and without the EOS model. The final

temperature for a particular element is similar for either model. However, the shock does

induce an initial temperature rise. As expected, the magnitude of this rise is larger on the

surface closest to the HE. The maximum increase in energy from the shock heating is approximately 0.1% of the total energy.
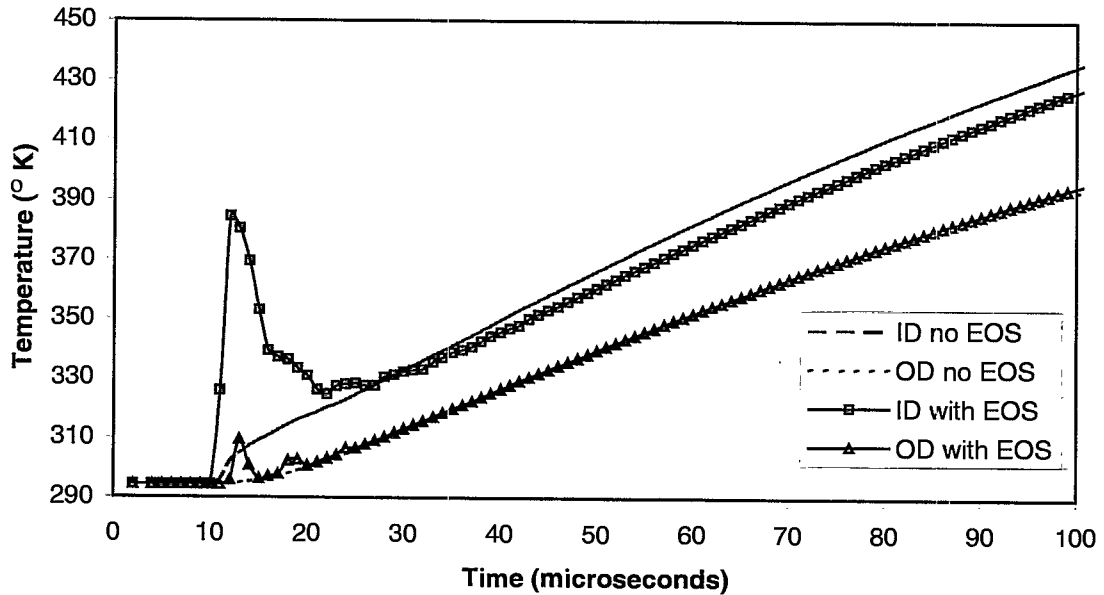

Figure 3.4: Temperature Effects from High Pressure Shock and Plastic Work

Early literature from Taylor (1963a) indicated that the hoop stress on the ID remains compressive after the hoop stress on the OD becomes tensile. This effect is illustrated in Figures 3.5 and 3.6. The hoop stress on the OD becomes tensile after 25 microseconds while the hoop stress on the ID becomes tensile after 54 microseconds. The early oscillations shown in Figures 3.5 and even more apparently in Figure 3.6 are a result of the reverberating elastic stress waves in the material. Several authors including Taylor (1963a) have shown that the hoop stress on the inner surface remains compressive until internal pressure is equal to yield stress. The radial stress, which is not shown here, remains negative long after the shock waves have attenuated and is still negative after 100 microseconds.
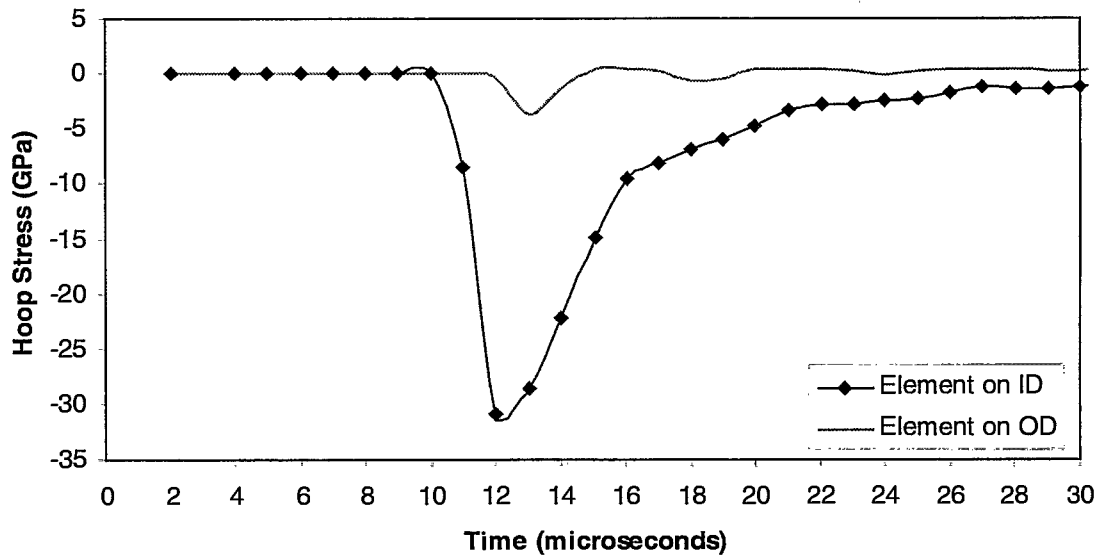
**Figure 3.5: Hoop Stress on the ID and OD of Expanding Ring
from 0-30 Microseconds**
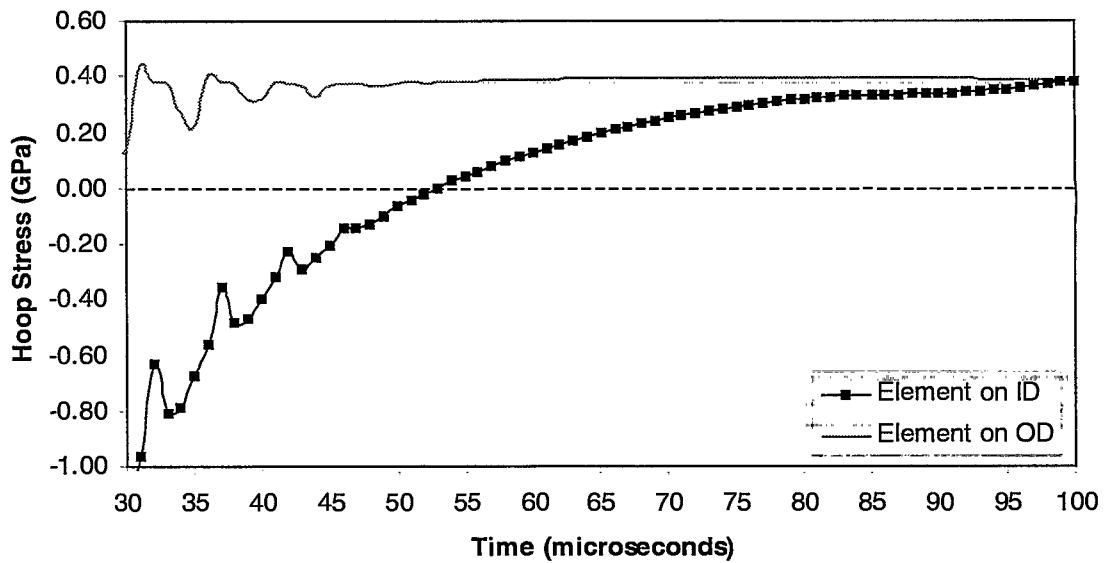
**Figure 3.6: Hoop Stress on the ID and OD of Expanding Ring
from 30-100 Microseconds**

The numerical model predicts a maximum shock velocity in the copper that is

approximately equal to the elastic wave speed. This indicates the presence of elastic

stress wave and most likely a combination of elastic and plastic stress waves due to the

magnitude of the loading. If the shock wave velocity was greater than the elastic wave

speed, a strong shock would propagate through the material as a single wave, which is shown for the case of P_3 in Figure 2.6.

The equivalent plastic strain rate for an element on the ID is shown in Figure 3.7. This figure indicates a maximum equivalent plastic strain rate of approximately 7.1×10^4 s^{-1} for calculations without the EOS and 6.6×10^4 s^{-1} for the calculations with the EOS subroutine. The equivalent plastic strain rate at 100 microseconds is 9.04×10^3 s^{-1} for calculations without the EOS and 9.18×10^3 s^{-1} for the calculations with the EOS model. The two curves are fairly close at this particular location on the mesh indicating that the EOS has a minor effect on the equivalent plastic strain rate. However, this observation is not conclusive in that the discrepancies between the two may be larger at other locations in the mesh and, as a result, additional comparisons should be performed.
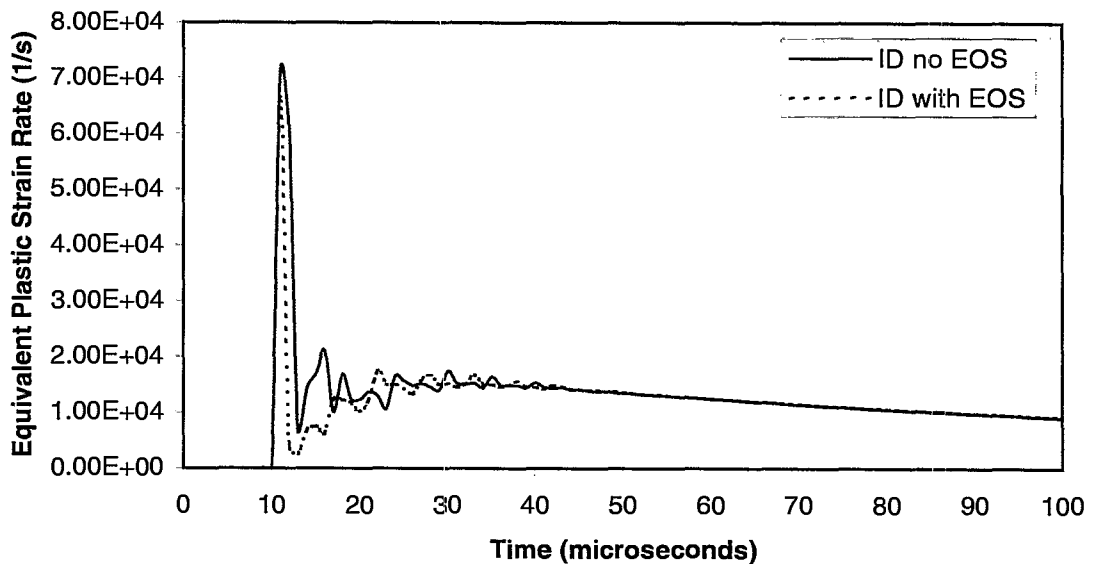
**Figure 3.7: Strain Rate on the ID with and without EOS Model**

The hoop strain for elements on the ID and OD with and without the EOS model is shown in Figure 3.8. From this figure, the strain on the OD is approximately the same

with and without the EOS model. However, the strain on the ID is slightly different which could be a result of compression in the shell material.
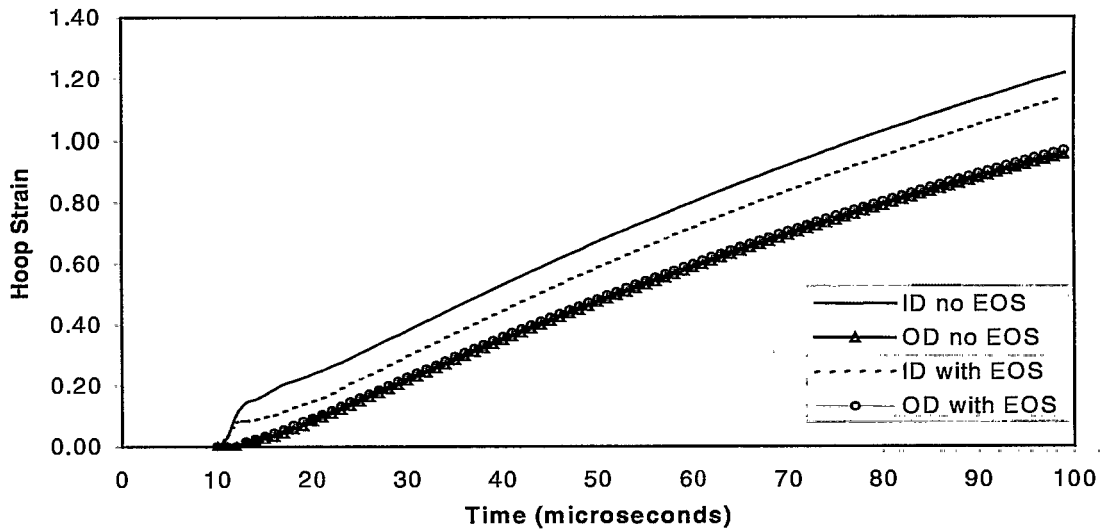
Figure 3.8: Hoop Strain with and without EOS Model

Finally, Figure 3.9 indicates the void volume fraction in the material for an element on the OD with and without the EOS model. The EOS model appears to have a minimal effect on this parameter. This trend is very similar for an element on the ID.
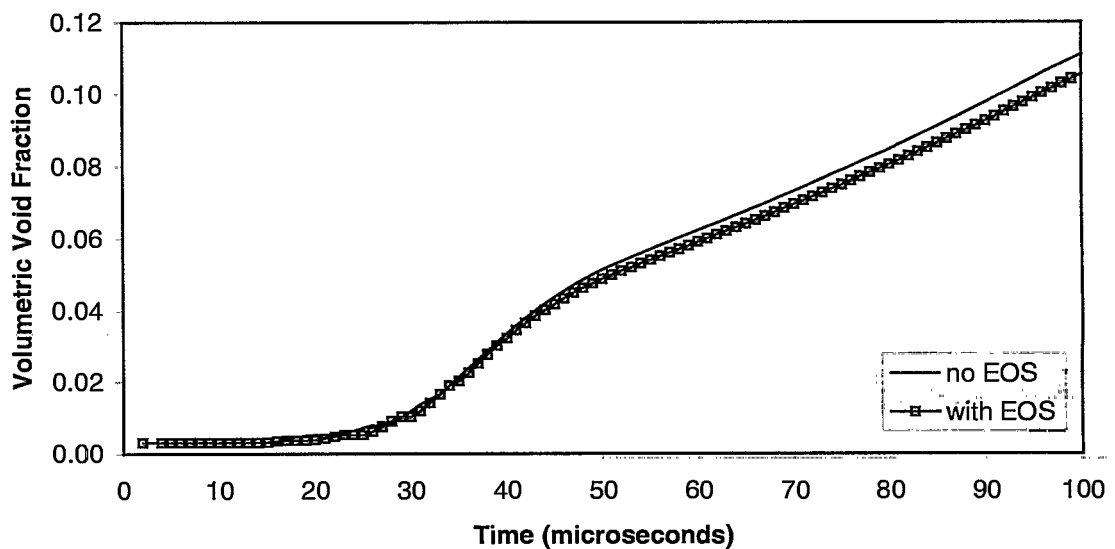
Figure 3.9: Void Volume Fraction on the OD with and without EOS Model